Open Research Online

The Open University's repository of research publications
and other research outputs

Characterization of the acidic cold seep emplaced jarositic Golden Deposit, NWT, Canada, as an analogue for jarosite deposition on Mars

Journal Item

How to cite:

Battler, Melissa M.; Osinski, Gordon R.; Lim, Darlene S. S.; Davila, Alfonso F.; Michel, Frederick A.; Craig, Michael M.; Izawa, Matthew R. M.; Leoni, Lisa; Slater, Gregory F.; Fairen, Alberto G.; Preston, Louisa J. and Banerjee, Neil R. (2012). Characterization of the acidic cold seep emplaced jarositic Golden Deposit, NWT, Canada, as an analogue for jarosite deposition on Mars. Icarus, 224(2) pp. 382–398.

For guidance on citations see FAQs.

© 2012 Elsevier Inc.

Version: Accepted Manuscript

Link(s) to article on publisher's website:
http://dx.doi.org/doi:10.1016/j.icarus.2012.05.015

Copyright and Moral Rights for the articles on this site are retained by the individual authors and/or other copyright owners. For more information on Open Research Online's data policy on reuse of materials please consult the policies page.

oro.open.ac.uk

Accepted Manuscript

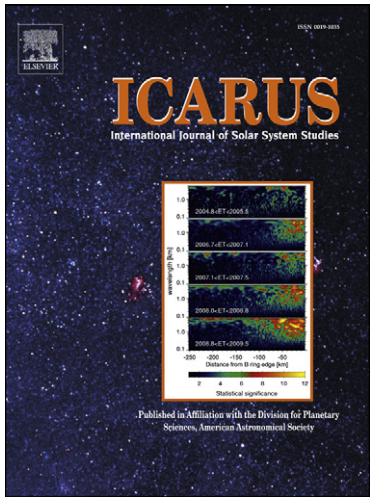

Characterization of the acidic cold seep emplaced jarositic Golden Deposit, NWT, Canada, as an analogue for jarosite deposition on Mars

Melissa M. Battler, Gordon R. Osinski, Darlene S.S. Lim, Alfonso F. Davila, Frederick A. Michel, Michael A. Craig, Matthew R.M. Izawa, Lisa Leoni, Gregory F. Slater, Alberto G. Fairén, Louisa J. Preston, Neil R. Banerjee

PII: S0019-1035(12)00189-3
DOI: http://dx.doi.org/10.1016/j.icarus.2012.05.015
Reference: YICAR 10222

To appear in: *Icarus*

Please cite this article as: Battler, M.M., Osinski, G.R., Lim, D.S.S., Davila, A.F., Michel, F.A., Craig, M.A., Izawa, M.R.M., Leoni, L., Slater, G.F., Fairén, A.G., Preston, L.J., Banerjee, N.R., Characterization of the acidic cold seep emplaced jarositic Golden Deposit, NWT, Canada, as an analogue for jarosite deposition on Mars, *Icarus* (2012), doi: http://dx.doi.org/10.1016/j.icarus.2012.05.015

This is a PDF file of an unedited manuscript that has been accepted for publication. As a service to our customers we are providing this early version of the manuscript. The manuscript will undergo copyediting, typesetting, and review of the resulting proof before it is published in its final form. Please note that during the production process errors may be discovered which could affect the content, and all legal disclaimers that apply to the journal pertain.

ACCEPTED MANUSCRIPT

Characterization of the acidic cold seep emplaced jarositic Golden Deposit, NWT, Canada, as an analogue for jarosite deposition on Mars

Melissa M. Battler[a,*], Gordon R. Osinski[a,b], Darlene S. S. Lim[c,d], Alfonso F. Davila[c,d], Frederick A. Michel[e], Michael A. Craig[a], Matthew R. M. Izawa[a], Lisa Leoni[f], Gregory F. Slater[f], Alberto G. Fairén[c,d], Louisa J. Preston[a], and Neil R. Banerjee[a]

[a]*Centre for Planetary Science and Exploration, Dept. of Earth Sciences, University of Western Ontario, 1151 Richmond St., London, ON, Canada, N6A 5B7*

[b]*Dept. of Physics and Astronomy, University of Western Ontario, 1151 Richmond St., London, ON, Canada, N6A 5B7*

[c]*NASA Ames Research Center, Mail-Stop 245-3, Moffett Field, CA, USA 94035*

[d]*SETI Institute189 Bernardo Ave., Suite 100, Mountain View, CA, 94043 USA*

[e]*Institute of Environmental Science, 2240 Herzberg Bldg., Carleton University, 1125 Colonel By Dr., Ottawa, ON, Canada, K1S 5B6*

[f]*School of Geography and Earth Sciences, McMaster University, 1280 Main St. West, Hamilton, ON, Canada, L8S 4K1*

[*]Corresponding author.
Tel.: +15192665036; fax: +15196613198. E-mail address: mbattle@uwo.ca (Melissa M. Battler).

Keywords: Mars, Geological processes, Mineralogy, Spectroscopy, Astrobiology

ACCEPTED MANUSCRIPT

ACCEPTED MANUSCRIPT

ABSTRACT

Surficial deposits of the OH-bearing iron sulfate mineral jarosite have been observed in several places on Mars, such as Meridiani Planum and Mawrth Vallis. The specific depositional conditions and mechanisms are not known, but by comparing martian sites to analogous locations on Earth, the conditions of formation and, thus, the martian depositional paleoenvironments may be postulated. Located in a cold semi-arid desert ~100 km east of Norman Wells, Northwest Territories, Canada, the Golden Deposit (GD) is visible from the air as a brilliant golden-yellow patch of unvegetated soil, approximately 140 m x 50 m. The GD is underlain by permafrost and consists of yellow sediment, which is precipitating from seeps of acidic, iron-bearing groundwater. On the surface, the GD appears as a patchwork of raised polygons, with acidic waters flowing from seeps in troughs between polygonal islands. Although UV-Vis-NIR spectral analysis detects only jarosite, mineralogy, as determined by X-Ray Diffraction and Inductively Coupled Plasma Emission Spectrometry, is predominantly natrojarosite and jarosite, with hydronium jarosite, goethite, quartz, clays, and small amounts of hematite. Water pH varies significantly over short distances depending on proximity to acid seeps, from 2.3 directly above seeps, to 5.7 several m downstream from seeps within the deposit, and up to 6.5 in ponds proximal to the deposit. Visual observations of microbial filament communities and phospholipid fatty acid analyses confirm that the GD is capable of supporting life for at least part of the year. Jarositic-bearing sediments extend beneath vegetation up to 70 m out from the deposit and are mixed with plant debris and minerals presumably weathered from bedrock and glacial till. This site is of particular interest because mineralogy (natrojarosite, jarosite, hematite, and goethite) and environmental

ACCEPTED MANUSCRIPT

conditions (permafrost and arid conditions) at the time of deposition are conceivably analogous to jarosite deposits on Mars. Most terrestrial analogues for Mars jarosites have been identified in temperate environments, where evaporation rates are very high and jarosites form along with other sulfates due to rapid evaporation (e.g. Rio Tinto, Spain; Western Australian acidic saline lake deposits). The GD is a rare example of an analogue site where jarosite precipitates under dominant freezing processes similar to those which could have prevailed on early Mars. Thus, the GD offers a new perspective on jarosite deposition by the upwelling of acidic waters through permafrost at Meridiani Planum and Mawrth Vallis, Mars. The GD also demonstrates that martian deposits may show considerably more chemical and mineral variability than indicated by the current remote sensing data sets.

1. Introduction

Mars today is a cold, dry planet, and most of the surface consists of permafrost (Carr and Schaber, 1977), which is defined as ground that remains at or below 0°C for at least two years (Harris et al., 1988). Liquid H_2O (water) is unstable on the surface for long periods of time under current atmospheric conditions, but substantial deposits of ground ice are hypothesized to occur within a depth of 1 m in circumpolar latitudes (Mitrofanov et al., 2003). A variety of observations support the existence of ice in the martian subsurface, including the detection of near-surface ground ice in martian northern latitudes by the Phoenix lander (Smith et al., 2009), and the Mars SHAllow RADar (SHARAD) sounder onboard Mars Reconnaissance Orbiter (MRO; Phillips et al., 2008).

ACCEPTED MANUSCRIPT

Despite the lack of water on Mars' surface today, past and present missions have observed minerals consistent with long-term crustal interaction with liquid H_2O, including phyllosilicates, hydrous sulfates, and halides (e.g., Bibring et al., 2006; Squyres et al., 2004b). Many scenarios for conditions on early Mars have been proposed, ranging from a cold, dry, but locally wet Mars (e.g., Carr and Head, 2003; Christensen, 2008; Ehlmann et al., 2011; Johnson et al., 2008) to a cold Mars with a cold (Parker et al., 1993) or glacially bound ocean (Fairén et al., 2011), to a warmer Mars, with warm oceans (Chevrier et al., 2007; Pollack et al., 1987). There is no consensus on what Mars' climate was like during the time these minerals were deposited, but recent studies suggest temperatures may have hovered around the freezing point of water (Fairén, 2010; Johnson et al., 2008). Even if we take a conservative approach and assume that conditions were indeed relatively cold and dry with local transient surface water, phyllosilicates, hydrous sulfates, and halides could have precipitated (Christensen, 2008; Ehlmann et al., 2011).

Of particular interest are the discoveries of layered deposits containing the OH-bearing Fe-sulfate mineral, jarosite, throughout Meridiani Planum (Christensen et al., 2004; Klingelhofer et al., 2004; Squyres et al., 2004b), and in several patches at Mawrth Vallis (Farrand et al., 2009; Michalski and Niles, 2011). Jarosite is thermodynamically stable under a majority of temperature and pressure conditions on present-day Mars (Navrotsky et al., 2005; Cloutis et al., 2008). As such, provided it has not recrystallized or decomposed, jarosite may contain chemical or textural indicators of Mars' history, perhaps including evidence of biological activity via ^{34}S isotopic composition (Navrotsky et al., 2005). Global mapping has revealed that similar sulfate-bearing mineralogical

ACCEPTED MANUSCRIPT

assemblages are widespread over the martian surface (Bibring et al., 2006). The layered deposits in Meridiani Planum have been interpreted as evidence for past upwelling and evaporation of acidic groundwater or surface water (Squyres et al., 2004b; Squyres et al., 2006), likely during the late Noachian (Andrews-Hanna et al., 2010; Hurowitz et al., 2010). Based on the wide distribution of sulfate deposits, acid sulfate aqueous systems could have directed the geochemistry of surface waters for extended periods of time during the late Noachian, either globally (Bibring et al., 2007; Fairén et al., 2004), or in isolated locations (Christensen, 2008). This places constraints on the type of mineral deposits that could have precipitated and also on the habitability of surface waters during that period of time.

A major question related to the martian acidic deposits is their mode of formation. Jarosite deposition requires acidic waters and oxidizing conditions. Natural acidic surface water systems most commonly occur on Earth in two types of settings. The first type is volcanic, where gases including H_2S and SO_2 are dissolved and oxidized in caldera lakes or hot springs (Varekamp et al., 2000; Zolotov and Shock, 2005). However, neither Meridiani Planum nor Mawrth Vallis are situated near enough to volcanoes, so this type of setting was not likely responsible for jarosite deposition. The second type is in areas where iron sulfide minerals are oxidized. Several terrestrial jarosite-rich sites of this formation nature have been described as analogues for Mars. For example, Rio Tinto, Spain (Amils et al., 2007; Bucky et al., 2003; Fairén et al., 2004; Fernández-Remolar et al., 2005), the Goldfield Au-Ag mining district, Nevada (Papike et al., 2006), Western Australian acidic saline lake deposits (Benison and LaClair, 2003; Baldridge et al., 2009), and Eagle Plains, Yukon, Canada (Lacelle and Léveillé, 2010). Many of these sites and

ACCEPTED MANUSCRIPT

most models developed to explain their martian counterparts invoke heating, or at the very least warm climates, for jarosite precipitation (e.g., Zolotov and Shock, 2005). More recently, however, analogue sites and mechanisms have been reported in cooler climates, with average annual temperatures below freezing (e.g., Lacelle and Léveillé, 2010; Michalski and Niles, 2011). This suggests the possibility of jarosite production under colder conditions, closer to those currently prevailing on Mars. Although surface temperatures during jarosite deposition at Meridiani Planum and Mawrth Vallis are not known with certainty, it is important to consider analogue sites in colder settings, with environmental properties representative of a colder Mars. These properties include prevailing freezing temperatures, frozen soils forming a thick layer of permafrost, and semi-arid to arid climate regimes (Fairén, 2010; Fairén et al., 2009).

In addition, if the deposits formed in an environment where evaporation dominated, the resulting geochemical conditions and the mineral phases that precipitate would have been different from an environment dominated by freezing and sublimation (Lacelle and Léveillé, 2010). Distinguishing one from the other would help constrain climate models of Early Mars and also habitability models of surface aqueous environments. Lacelle and Léveillé (2010) determined through modeling and ground truthing that mineral assemblages at Eagle Plains were produced by freezing, rather than evaporation. The same techniques could be applied to other cold-climate acidic aqueous systems. The polar regions of Earth present some of the most relevant analogue science opportunities for ground truthing models and evaluating hypotheses concerning physicochemical processes on Mars (e.g., High Lake gossan deposit in Nunavut, Canada (West et al., 2009); Eagle Plains, Yukon, Canada (Lacelle and Léveillé, 2010)). The

ACCEPTED MANUSCRIPT

Golden Deposit (GD), Northwest Territories, Canada (Michel and van Everdingen, 1987), features jarosite and other sulfates precipitating from cold acidic groundwater seeps and is of particular interest as analogous martian features may have been produced through similar processes. Here, we report on the first detailed field, mineralogical, and geochemical characterization of the GD. Table 1 compares temperature and precipitation, along with additional properties of the GD, to Meridiani Planum and Mawrth Vallis, Mars, and other terrestrial analogue sites.

1.1. The Golden Deposit

The Golden Deposit (GD) is located in the Canadian Arctic ~100 km east of Norman Wells, Northwest Territories (65º11'58" N, 124º38'15" W; Fig. 1). It is visible from the air as a golden-yellow patch of unvegetated soil approximately 140 m long × 50 m wide, within the muskeg-rich boreal forest typical of the subarctic taiga. It was discovered in 1975 and referenced as the "Golden Deposit" by Michel (1977). The surface of the GD features an interconnected network of 1–3 m diameter raised polygons (Figs. 2a, b). Water flows in small channels within the troughs between polygons.

The GD consists of an accumulation of yellow ochre, precipitating from numerous closely spaced seeps in troughs. Seeps deliver cold, acidic, iron-bearing waters from the sub-surface, and can be identified by slow streams of small bubbles. In most cases flow rates are very low, at approximately 2 to 3 L/min (Michel and van Everdingen, 1987). The seeps range in diameter from roughly several mm to 20 cm across, can be 10

ACCEPTED MANUSCRIPT

or more cm deep, and vary in appearance from discreet holes in sediment (Fig. 2i) to obvious deep holes within channels (Fig. 2i), to "craters", up to 1 m in diameter. The GD is bounded on the west by a shale outcrop in the form of a small hill, and on the southwest and southeast by Ponds 1 and 2 (Fig. 1). In other directions the GD is surrounded by older deposits produced by the same system, which are now buried beneath muskeg. Water flows in a predominant northwest to southeast direction across the GD, and exits into a pond at the southeast end (Pond 2, Fig. 1). Small ponds along the perimeter on the north and west sides may receive some active layer seepage flow from higher ground, and these ponds provide the source for surface water, which mixes with seep water and flows northwest to southeast across the deposit. Microbial filaments are present in a few of the troughs (Figs. 2g, h) and a few insects were observed swimming in channels.

The GD is underlain by unit "C" of Yorath and Cook (1981), which is a thick sequence of Cretaceous pyritiferous marine shales deposited within the Great Bear Basin. This unit also outcrops immediately to the west of the GD. In this area unit "C" has a thickness of up to 250 m. Approximately 100 m of shale (units A and B) underlie unit C. Below these shales are Devonian to Cambrian age rocks, with Precambrian rocks below that. The surface of the GD is sporadically strewn with boulders (tens) and cobbles (hundreds) of widely varying composition. These may have been emplaced as till during the last glaciation and have undergone frost heave up through what is now the GD. Zero to 50 m of quaternary sediments may still underlay the GD. Michel and van Everdingen (1987) determined the deposit to be at least 1 m thick, but could not penetrate deeper due to permafrost, which is widespread but discontinuous throughout the entire region below

ACCEPTED MANUSCRIPT

approximately 1–2 m depth in the fall (Rühland and Smol, 1998). Evidence of permafrost underlying the GD includes: 1. the development of polygonal patterns on the surface of the deposit; 2. the presence of a frozen zone at depth, encountered by a push core; and 3. the presence of several small raised peat palsas in the organic-rich material immediately south of the deposit, presumed to be ice-cored. The depth of GD sediment overlying the Cretaceous shale unit is unknown, and the presence of till overlaying the shale and underlying the GD has yet to be directly confirmed. Assuming the total thickness of the GD is not more than 2–3 meters, it is likely situated primarily within the active layer. Although the deposit appears to be muddy, it is firm enough to walk on.

Michel (1977) identified the soil composition to be jarositic, and suggested that the acid seep waters form through reactions of ground water first with dolomite, and then with a pyritiferous shale bed at depth. Sulfur isotope work presented by Michel and van Everdingen (1987) shows that sulfur in the sulfate minerals, including the jarosite, originates from sulfide (highly negative values of -19 to -25 ‰). As water flows through rocks at the hypothesized recharge site, dissolution of dolomite results in groundwater with an initial composition rich in Ca^{2+}, Mg^{2+} and HCO_3^-. Water then flows through the pyritiferous shale beds underlying the GD, and $Ca^{2+} + Mg^{2+}$ for $Na^+ + K^+$ cation exchange occurs. Na^+ and K^+ are assumed to originate from clay minerals in the shale beds. Oxidation of pyrite also takes place in the subsurface, long before water reaches the surface at discharge. Oxygen in the water (both in the structure and dissolved) are the source for the sulfates (van Everdingen et al., 1985). These reactions result in high concentrations of iron, sulfate, and hydrogen ions. HCO_3^- ions are consumed to form carbonic acid and the liberated iron and sulfate ions interact with K^+ and Na^+ to produce

ACCEPTED MANUSCRIPT

jarosite (Michel and van Everdingen, 1987). Biochemical oxidation of pyrite is thought to play a role, and may be accelerated by iron-oxidizing bacteria, such as *Thiobacillus ferrooxidans* (van Everdingen et al., 1985). The suspected recharge area for the flow system is located 12 km to the west and features outcrops of, and sinkholes in, Lower to Middle Devonian and Ordovician limestones and dolostones along a 300 m high ridge representing the Keele Arch (an anticlinal structure with a thrust fault at the base of the ridge). Tritium dating of the water by Michel (1977) indicates that the water has an average residence time in the subsurface of approximately 15 years before discharging.

Weather data have been collected in Norman Wells over the past 30 years. Environment Canada (2010a) reports a mean annual air temperature of -5.52 °C, and maximum and minimum air temperatures of 35 °C and -52 °C, respectively. Mean annual precipitation for Norman Wells is 290 mm (Environment Canada, 2010a), and thus the area may be defined as a cold semi-arid desert (Warner, 2004). It is not known whether the seeps flow year round, as they have never been visited during the winter. It is possible that they become inactive during the winter months when the active layer freezes.

2. Field sampling

In September 2008 a two-day field campaign to the GD was undertaken with the goals of mapping the physical and chemical conditions of the surface deposits and collecting samples. Sediment samples were collected in and around the GD for mineralogy, major and trace element, and spectral analyses. Mineralogy samples were selected to determine detailed spatial mineralogy trends and variability, elemental

ACCEPTED MANUSCRIPT

239 analysis was determined to support mineral identification, and spectral analyses were
240 used to establish whether all minerals can be observed via remote sensing. Water samples
241 were also collected to expand upon water chemistry data presented by Michel and van
242 Everdingen (1987). Five sites within the GD and a pond to the southeast were selected to
243 be sampled for mineralogy and water chemistry (GD Sites 1–5, Pond 2; Fig. 1).
244 Sediments at many additional sites were sampled for mineralogy and spectral analysis, as
245 indicated in Figure 3 and described below.
246
247 *2.1. Sediment and mineral sample collection*
248
249 Seven categories of sediment and mineral samples were collected in and around
250 the GD: ochre, crust, core, terrace, transect, shale, and evaporite minerals. Yellow ochre
251 samples were collected from the upper 0.5 to 2 cm at various locations in and around the
252 GD including from Sites 1 to 5, and Pond 2 to the south of the GD, and were typically
253 wet upon collection (Figs. 2b, 3). Sample sites include various channels and pools
254 throughout the GD, including locations directly above seeps (Sites 2 and 3), and
255 downstream from seeps. Crust samples, representing drier surficial yellow ochre within
256 the GD, were taken as well from the raised centers of polygons (Fig. 2b). A core sample
257 was taken at Site 2, which was selected for its particularly low pH (2.78). A push core
258 was used to obtain a soil sample down to ~50 cm, and the core was sub-sectioned in the
259 field. It was not possible to penetrate past the active layer with the coring device and, as
260 such, samples within the permafrost zone were not recovered (Fig. 2c). Terrace samples
261 were collected from an area of flowing water where small, centimetre scale terraces have

ACCEPTED MANUSCRIPT

formed. These terraces were in most cases ridged with streamer-form microbial filaments (Figs. 2g, h). Transect samples were collected along several transects radially outward from the deposit into the surrounding muskeg to the north and east. Ponds 1 and 2 to the southwest and southeast of the GD (Fig. 1) and a small hill bounding the GD to the west prevented sampling of subsurface sediments in those directions. Shale samples were collected from the small hill to the west, which comprises a weathered shale outcrop largely blanketed by glacial till. Trenches dug into the weathered shale revealed patches of bright red, yellow, and orange soil (Fig. 2f). Evaporite minerals forming thin white coatings on grasses, mosses, organic rich mud, and leaves around the edge of the GD deposit were also sampled (Fig. 2e).

2.2. Water chemistry sampling

Water pH and temperature measurements were obtained in the field with a handheld instrument, and recorded at 73 locations throughout the deposit. Conductivity levels were measured using a Yellow Springs Instrument temperature, conductivity, and salinity meter, and were recorded at 35 locations.

Water chemistry samples were also collected from Sites 1 to 5 and from approximately 0.3 m water depth in Pond 2. Water sampling protocols followed those provided by the Environment Canada, Pacific Environmental Science Centre (PESC) in Vancouver, Canada. Unfiltered samples were collected in acid washed 250 and 500 mL bottles, rinsed four times with sample water, kept cool and dark for the duration of the field season, and then immediately shipped to the PESC labs for analysis. Filtered

ACCEPTED MANUSCRIPT

samples for metal and nutrient analyses were similarly kept cool and dark, and sent to PESC following the field season. Upon return to base camp, unfiltered samples were also measured for pH with a Hannah pH meter that was calibrated to buffers daily.

3. Analytical techniques

3.1. Mineralogy, X-ray diffraction

Samples were analysed to determine detailed spatial mineralogy trends and variability. All sediment samples were air dried for more than one month at room temperature. Most samples for X-ray diffraction (XRD) were crushed by hand with an alumina mortar and pestle, and dry sieved to < 53 µm. These samples were also used for spectral analysis. Additional samples for XRD analysis were crushed by hand with a stainless steel mortar and pestle. Detailed mineral determination was performed on 43 samples for this study via XRD (Co K-alpha radiation λ=1.7902 Å, Rigaku Rotaflex, 45kV, 160 mA, 2º-82º 2θ) at the Laboratory for Stable Isotope Science at the University of Western Ontario (Western), and crystalline mineral phases were identified using the International Center for Diffraction Data Powder Diffraction File (ICDD PDF-4) and the BrukerAXS Eva software package at the micro-XRD facility at Western. Qualitative relative abundances of minerals observed were determined based on visual inspection of peak height intensities. Minerals with peak height intensities >5000 are referred to as "major", and minerals with peak height intensities <5000 are considered "minor".

ACCEPTED MANUSCRIPT

3.2. Whole rock major and trace element analysis

Major and trace elements were determined to support mineral identification. Oxide and trace element abundances for 6 representative samples were determined by Acme Analytical Laboratories (Vancouver) Ltd. via inductively coupled plasma emission spectrometry (ICP-ES). Total abundances of the major oxides and several minor elements were reported in weight % or ppm on a 0.2g sample analysed by ICP-ES following a lithium metaborate/tetraborate fusion and dilute nitric acid digestion. Loss on ignition (LOI) is by weight difference after ignition at 1000°C. One sample each of ochre (GD-23) and crust (GD-10a) were analysed, as well as one sediment (ochre) sample from the surface of the acidic seep site where the core was extracted (GD-site2a), and one core sample from 40 cm depth (GD-site2f). One transect sample taken near the edge of the deposit (GD-T4a) and another transect sample approximately 40 m out from the edge of the deposit (GD-T4c) were also analysed.

3.3. Spectral analysis

Spectral analyses were used to establish whether all minerals seen with XRD can be observed via remote sensing. Spectra of 48 samples powdered to <53 µm were collected with a FieldSpec Pro HR spectrometer at the University of Winnipeg Planetary Spectroscopy Facility (Cloutis et al., 2006a). 0.35-2.5 µm spectra were acquired at i = 30º, e = 0º relative to Spectralon® with an ~5 mm field-of-view, using a 50 watt quartz-

ACCEPTED MANUSCRIPT

tungsten-halogen light source; 500 spectra were averaged to increase the signal-to-noise ratio.

3.4. Water chemistry

A total of 44 environmental variables were measured for the 6 water samples by PESC, including: major ions (Ca^{2+}, Mg^{2+}, K^{+}, Na^{+}, S^{2-}, Cl^{-}, F^{-}, SO_4^{2-}), metals (Al, Sb, As, Ba, Be, B, Cd, Cr, Co, Cu, Fe, Pb, Mn, Mo, Ni, Se, Ag, Sr, Sn, Ti, V, Zn), pH, alkalinity, hardness, conductivity, nitrogen (NH_3, NO_3, NO_2, total nitrogen), phosphorus (total unfiltered P, total dissolved P, PO_4^{3-}), carbon (dissolved inorganic C, dissolved organic C), and Si. Twenty four environmental variables are reported here.

4. Results

4.1. Mineralogy

GD mineralogy results from XRD are presented as a map in Figure 4. Major minerals include natrojarosite (the sodium end-member of jarosite, ($NaFe^{3+}{}_3(SO_4)_2(OH)_6$)), jarosite (the potassium end-member, which is referred to throughout this paper simply as jarosite, ($KFe^{3+}{}_3(SO_4)_2(OH)_6$)), hydronium jarosite (($(H_3O)Fe^{3+}{}_3(SO_4)_2(OH)_6$), quartz ($SiO_2$), goethite ($Fe^{3+}O(OH)$), and gypsum ($CaSO_4{\cdot}2H_2O$). Minor minerals include hematite (Fe_2O_3), plagioclase ($(Na,Ca)(Si,Al)_4O_8$), rutile (TiO_2), muscovite ($KAl_2(Si_3Al)O_{10}(OH,F)_2$), illite

ACCEPTED MANUSCRIPT

353 ($(K,H_3O)(Al,Mg,Fe)_2(Si,Al)_4O_{10}[(OH)_2,(H_2O)]$), gismondine ($Ca_2Al_4Si_4O_{16}\cdot 9(H_2O)$),
354 ferrihydrite ($Fe_5O_7(OH)\cdot 4H_2O$), anhydrite ($CaSO_4$), hexahydrite ($MgSO_4\cdot 6H_2O$),
355 thenardite (Na_2SO_4), vauxite ($Fe^{2+}Al_2(PO_4)_2(OH)_2\cdot 6(H_2O)$), fibroferrite
356 ($Fe^{3+}(SO_4)(OH)\cdot 5(H_2O)$), alunogen ($Al_2(SO_4)_3\cdot 17H_2O$), nacrite ($Al_2Si_2O_5(OH)_4$), and
357 douglasite ($K_2Fe^{2+}Cl_4\cdot 2H_2O$). In addition, very small amounts of various clays, including
358 vermiculite ($(Mg,Fe,Al)_3(Al,Si)_4O_{10}(OH)_2\cdot 4(H_2O)$) and kaolinite ($Al_2Si_2O_5(OH)_4$), as
359 well as amphibole (E.g., $Ca_2(Mg,Fe,Al)_5(Al,Si)_8O_{22}(OH)_2$) are present in most samples
360 (Table 2, Fig. 4).

361 Overall, natrojarosite and jarosite dominate the majority of samples. The d-
362 spacing values for crust sample GD-12, which includes natrojarosite, jarosite, and
363 hydronium jarosite are: 3.11 Å (100 % intensity, $2\theta = 33.38$ °), 3.07 Å (98.4 % intensity,
364 $2\theta = 33.89$ °), 5.07 Å (85.5 %, $2\theta = 20.31$ °), 1.98 Å (34.1 % intensity, $2\theta = 53.79$ °),
365 1.83 Å (31.3 %, $2\theta = 58.56$ °), and others with decreasing intensities.

366

367 *4.1.1. Ochres*

368

369 Analyses of the 11 ochre samples confirmed the predominance of natrojarosite
370 and jarosite in all samples, with major hydronium jarosite in 5 samples, and minor
371 gypsum and hematite in 4 samples, 3 of which are associated with the hydronium
372 jarosite-bearing samples, and also contain minor clay minerals including illite. Minor
373 goethite is present in all samples, along with varying abundances of quartz. Minor
374 muscovite and rutile are present in 9 samples, and minor plagioclase feldspar is found in

ACCEPTED MANUSCRIPT

4 samples (Table 2, Figs. 2b, 4). Hydronium jarosite, gypsum, hematite, and illite are associated with some of the most acidic sample sites.

4.1.2. Crusts

The 4 surficial "crust" samples (top 5 mm) contain natrojarosite in all samples, jarosite in 3 samples, goethite in the sample lacking jarosite, and minor goethite in the 3 jarosite-bearing samples. Varying amounts of quartz are present in all 4 samples, along with minor muscovite in 3 samples, feldspar in 2 samples, and rutile in 1 sample (Table 2, Figs. 2b, 4).

4.1.3. Core

Sediments within the core were mostly comprised of a homogeneous yellow-ochre, similar in appearance to the surface of the GD. The 4 core samples contain natrojarosite, jarosite, and hydronium jarosite, with minor hematite, goethite and gypsum in the upper 3 samples, and larger amounts in the deepest sample. Minor quartz is present in the upper 2 samples, with more quartz in the lower 2. Minor rutile, muscovite, and illite are present in all samples, and minor plagioclase is found in the deepest 2 samples (40 and 50 cm). Goethite, gypsum, and hematite abundances increase with depth, with the relative amount of jarosite decreasing with depth. Quartz and plagioclase abundances also increase with depth. A layer of sandy gravel was observed at approximately 45 cm depth (Table 2, Figs. 2c, 4).

ACCEPTED MANUSCRIPT

398

399 *4.1.4. Terraces and microbial filaments*

400

401 The single sediment sample from a terrace (GD-20) contains natrojarosite and
402 quartz, with minor jarosite, goethite, plagioclase, rutile, and muscovite. The single
403 sample of a sediment-coated streamer (biofilament; GD-19) has nearly the same
404 mineralogy, differing only in increased quartz abundance, and decreased natrojarosite
405 abundance (Table 2, Figs. 2g, h, 4).

406

407 *4.1.5. Transects*

408

409 Samples and test pits from transects show that jarositic sediments extend beneath
410 the vegetation out to a radius of 20 to 30 m away from the main deposit to the west and
411 north, and up to 70 m away to the east. These sediments persist to a depth of roughly 50
412 cm, and are mixed with organic debris (peat, plant matter). Mineral abundances vary
413 greatly. Most samples contain jarosite, 6 contain natrojarosite, 7 contain hydronium
414 jarosite (4 of these also contain natrojarosite, and 2 contain gypsum), nearly all samples
415 contain minor goethite, three contain gypsum, three contain hematite, one contains
416 ferrihydrite ($Fe_5O_7(OH)\cdot 4H_2O$), and one contains anhydrite. Most samples include
417 significant quartz and minor plagioclase, rutile, and muscovite, and four samples contain
418 gismondine. There is a general decrease in natrojarosite, jarosite, and goethite with
419 distance from the GD. Gypsum and ferrihydrite appear furthest out from the GD, and

ACCEPTED MANUSCRIPT

quartz and feldspars generally appear in increasing abundances further from the deposit (Table 2, Figs. 2d, 4).

4.1.6. Evaporitic salt crusts on vegetation

Of the 3 samples of evaporated minerals on plant leaves and soil, 2 contain only gypsum, and the other contains significant proportions of the sulfates thenardite (Na_2SO_4) and hexahydrite ($MgSO_4 \cdot 6H_2O$), as well as minor gypsum, vauxite ($Fe^{2+}Al_2(PO_4)_2(OH)_2 \cdot 6(H_2O)$), and fibroferrite ($Fe^{3+}(SO_4)(OH) \cdot 5(H_2O)$; Table 2, Fig. 2e).

4.1.7. Shale

The 5 samples of the shale unit outcropping immediately west of the GD (pyrite-bearing unit "C"; Yorath and Cook, 1981) are composed largely of quartz, clay minerals and small amounts of jarosite. Weathered yellow patches within the shale are composed of quartz, jarosite, goethite, muscovite mica, and possibly alunogen ($Al_2(SO_4)_3 \cdot 17H_2O$), nacrite ($Al_2Si_2O_5(OH)_4$), and douglasite ($K_2Fe^{2+}Cl_4 \cdot 2H_2O$). Weathered orange patches contain quartz, jarosite, and mica, and red patches are composed of quartz, possible nacrite, mica, hematite, goethite, rutile, feldspar, and clay minerals (Table 2, Figs. 2f, 4). Pyrite was not detected, although it is known from drill core collected by oil companies to be present elsewhere in this unit (Yorath and Cook, 1981).

4.2. Whole rock major and trace element analysis

ACCEPTED MANUSCRIPT

443

444 The most abundant major elements (expressed as oxides), forming approximately
445 68% by mass of most samples, are Fe_2O_3, SiO_2, K_2O, Na_2O and Al_2O_3 (Table 3). All
446 samples contain a large amount of Fe_2O_3 (19 to 50 %), with elevated abundances at the
447 acidic seep site, and reduced amounts with distance from the GD. SiO_2 is the next most
448 abundant oxide, and its content increases with distance from the GD, and is lowest at the
449 acidic seep site. As with Fe_2O_3, K_2O is present in greater quantities at the acidic seep site,
450 and in reduced quantities with distance from the GD. Na_2O differs from all other oxides
451 in that abundances are neither increased nor reduced at the acidic seep site, but are
452 slightly elevated in the ochre and crust sediment samples. Like Fe_2O_3 and K_2O, Na_2O
453 decreases with distance from the deposit. Like SiO_2, all other major element oxides
454 (Al_2O_3, MgO, CaO, TiO_2, P_2O_5, MnO, and Cr_2O_3) increase in concentration with distance
455 from the GD, and generally decrease at the acidic seep site. Most trace element
456 concentrations increase with distance from the GD (Ba, Sr, Zr, Y, Sc), and decrease at the
457 acidic core sample site, except Ni and Nb, which have increased abundances at the acidic
458 core sample site. Total C increases with distance from the GD, and decreases at the acidic
459 core sample site, and in the dried surficial crust. Total S is slightly elevated above the
460 acidic seep site, and decreases with distance from the GD. Calculations using this data
461 indicate that normative jarosite constitutes approximately 48 weight % of two
462 representative ochre (GD-23) and crust (GD-10a) samples, and approximately 28 weight %
463 of a transect (GD-T4a) sample.

464

465 *4.3. Spectral analysis*

ACCEPTED MANUSCRIPT

ACCEPTED MANUSCRIPT

Ultraviolet-visible-near-infrared (UV-Vis-NIR) reflectance spectra were acquired on 48 of the sediment samples. Results confirm that the GD is dominated by jarosite and natrojarosite. Given the relative spectral brightness and depth of the Fe^{3+} absorption features in jarosite/natrojarosite, other mineral phases are largely masked. Other mineral phases can, however, be seen in spectra of a few individual samples; particularly those containing hematite/goethite. Both jarosite and natrojarosite can be identified by their characteristic absorption features associated with Fe^{3+} and overtones of the vibrational features of OH and S-O bonds. While distinguishing the two is possible in high resolution laboratory spectra, spectra of the two obtained remotely would likely result in the two being spectrally indistinguishable. The absorption features from 0.4 to ~ 1.3 μm are produced by Fe^{3+} $^6A_{1g}$ spin-forbidden ligand field transitions in iron atoms that are linked through edge or corner-shared Fe^{3+} $(O/OH)_6$ octahedra (Rossman, 1976; Sherman and Waite, 1985). In both jarosite types, Fe^{3+} absorption bands with minima at ~0.43, 0.50, 0.63 and 0.92 μm are a result of these transitions. The absorptions at 1.47 and 1.53 μm are attributed to 2νOH overtones of O-H stretching fundamentals occurring from 2.80-3.15 μm, while the absorptions from ~ 1.80 through 2.50 μm are the result of combinations of the overtones of OH stretching, adsorbed H_2O stretching and O-S-O bending fundamentals (Cloutis et al., 2006b).

The acquired spectra of the GD samples are all point spectra of samples prepared as detailed in the analytical techniques section. As such, individually they are not representative of the whole site. To produce a spectrum akin to that which would be acquired by an orbital instrument we have produced a representative spectrum via a linear

ACCEPTED MANUSCRIPT

mixture of the spectra of 21 of the surficial samples collected. This spectrum contains features only of natrojarosite, despite the fact that some of the individual spectra contained features of other minerals.

4.4. Water chemistry

Water pH measurements taken *in situ* vary from 2.2 to 5.7 within the deposit and up to 6.7 in Pond 2, southeast of the deposit. pH is correlated with seep sites, and often varies significantly over short distances depending on proximity to acid seeps. The most acidic waters occur directly above seep sources, and acidity typically decreases sharply downstream. For example, a pH of 2.2 was measured immediately above one seep, and several metres downstream pH was 5.2. pH is lowest toward the southwest edge of the deposit, and is higher in small ponds surrounding the GD. In general, pH increases to nearly neutral along transects radially outward from the deposit (Fig. 5a, Table 4). However, a few sites with pH measurements of 2.2 to 4.0 were identified up to approximately 40 m distance from the deposit. In addition, water samples were taken from each of the 5 main Sites, as well as Pond 2 at the southeast outflow of the deposit, and pH was measured back at base camp at the end of the day. By this method, pH was found to be lowest at Sites 2 and 3, at 2.8 and 3.1, respectively, and highest at Site 4 (5.2) and Pond 2 (6.7).

Water temperatures measured *in situ* vary independently from pH, and range from 2.8 ºC to 10.2 ºC. Maximum temperatures were recorded at the north end of the GD (up to 10.2 ºC), and the southwest edges of the deposit, in and around Pond 1 (up to 10.0 ºC).

ACCEPTED MANUSCRIPT

In general, temperatures are highest in association with seeps, and at the edge of the deposit, decreasing slightly inside the deposit (down to ~6.0 ºC), and decreasing significantly with radial distance outward from the deposit to a minimum of 2.8 ºC (Fig. 5b). Conductivity values, also measured *in situ*, range from 0.01 to 10.3 mS/cm, and trends do not seem to be correlated with seep site location, as maximum, minimum, and moderate conductivity values were all measured at seep sites (Fig. 5c). Conductivity is generally lowest in the middle of the deposit, and higher around the edge of the deposit.

Water chemistry results are shown in Table 4. Hardness (dissolved total calcium) and conductivity are both highest at Site 2 (3370.0 mg/L and 6300.0 µS/cm, respectively), followed by Site 3, then Pond 2, with minimum values at Site 5 (122.0 mg/L and 274.0 µS/cm, respectively). Of the major anions, SO_4^{2-} is most abundant, followed by S^{2-}. SO_4^{2-}, S^{2-}, and Cl^- anions follow the same patterns as hardness and conductivity, with greatest concentrations at Site 2 (4170.0 , 1596.01, and 18.3 mg/L, respectively) followed by Site 3, then Pond 2, with minimum values at Site 5 (111.0, 27.8, and 0.7 mg/L, respectively). Fluoride concentrations are less than 1 mg/L and do not follow this pattern. Of the major cations Mg^{2+} is most abundant, followed by Na^+ and Ca^{2+}. Magnesium, Ca^{2+}, and Na^+ also show the same pattern as most anions, with greatest amounts at Site 2 (475.0, 343.0, and 426.0 mg/L, respectively) followed by Site 3, then Pond 2, with minimum values at Site 5 (12.1, 14.9, and 2.9 mg/L, respectively). Potassium concentration differs slightly in that it is most abundant at Site 2 (20.1 mg/L), followed by Pond 2 (3.8 mg/L) and then Site 3 (0.9 mg/L), with a minimum value at Sites 4 and 5 (0.3 mg/L). Of the metal concentrations measured Fe is most abundant, followed by Al. Antimony, B, Mn, and Sr all have maximum concentrations of less than 5.0 mg/L, and follow the same trends as

ACCEPTED MANUSCRIPT

most of the major ions, with maximum values at Site 2, followed by Site 3, then Pond 2, with minimum values at Site 5. Aluminum and Fe do not follow the same pattern as major ions. Al is most abundant at Site 3 (16.9 mg/L) followed by Sites 1 and 4, with a minimum value at Site 5 (0.5 mg/L). Fe concentrations are highest at Sites 2 (309.0 mg/L), 5 (18.4 mg/L), and 3, and lowest at Site 4 (5.8 mg/L). Si is most abundant at Sites 3 and 2 (19.5 and 14.1 mg/L, respectively), and P and total N follow roughly the same trend as most major ions with maximum values of 2.8 and 15.3 mg/L, and minimum values of 0.2 and 0.9 mg/L. Dissolved inorganic C (DIC) and dissolved organic C (DOC) do not follow the same trends as anything else. DIC is most abundant at Pond 2 at 5.0 mg/L, and DOC is most abundant at Site 4 (22.9 mg/L) and Site 1 (17.2 mg/L).

In summary, Site 2 is most acidic, and in general richer in major ions, having the highest conductivity and hardness. Site 3 is the second most acidic location and has the second highest ion concentrations, conductivity, and hardness. From here, acidity and ionic concentrations (plus conductivity and hardness) diverge. pH increases from Site 3, through Sites 5, 1, and 4, and Pond 2 has the highest pH. Alkalinity trends follow those of pH. Ionic concentrations, conductivity, and hardness decrease from Site 3 to Pond 2, followed by Site 1, Site 4, and finally Site 5. The only metals and ions that do not follow these trends exactly are Al, Fe, K, and Si. Dissolved inorganic carbon is most abundant in Pond 2, consistent with highest alkalinity and pH. Dissolved organic carbon is most abundant at Sites 4, 1, and 3, which does not follow any other noted water chemistry pattern.

5. Discussion

ACCEPTED MANUSCRIPT

558

559 *5.1. Physical trends and implications for mineralogy and microbiology*

560

561 *5.1.1. Water pH and implications for mineralogy*

562

563 The sharp increases in pH noted with short distances from seep sites are likely due
564 to dilution by active layer water and consumption of hydronium by hydronium jarosite
565 and jarosite precipitation. Correspondingly, the greatest concentrations of hydronium
566 jarosite are found at the most acidic sites (Sites 2 and 3), in addition to illite, gypsum and
567 hematite. The latter two minerals are capable of forming under low pH conditions
568 (Zolotov and Shock, 2005), but are not restricted to low pH depositional environments.
569 Increased Na^{2+} and Ca^{2+} cations are also noted in water at Sites 2 and 3, and although Fe,
570 K^{+}, and S^{2-} are not elevated in water, Fe_2O_3, K_2O, and S are elevated in sediments at
571 these sites, suggesting K^{+} in water is being consumed in jarosite production. The pH may
572 be lowest toward the southwest edge of the deposit because this area does not lie along
573 the main flow path of the active layer water, which flows from the northwest stream to
574 the southeast pond. Therefore, acidic waters do not get as diluted here. It is also possible
575 that there are more seeps in this area, introducing more acidic water. In general, pH
576 increases radially outward from the deposit, somewhat correlating with decreasing
577 jarosite in soils. pH increase is most notable where seep waters are diluted with pond
578 water. The fact that a few sites with pH measurements of 2 to 4 were identified
579 approximately 30 m from the deposit suggests that there may still be a few active seep
580 sites beneath the vegetation. It is not known whether these are older seep sites still

ACCEPTED MANUSCRIPT

persisting, or if these are new seep sites, which may eventually kill off the overlying vegetation.

5.1.2. Temperature and conductivity trends

Maximum temperatures are measured in some of the deepest ponds at the north end and southwest corner of the GD, presumably because of increased thermal inertia due to water depth, and heating by sunlight. In general temperatures are higher around the edge of the deposit; perhaps due to shallow bodies of still water being heated by the sun. Temperatures are also higher than average at seep sites and in shallow streams, likely reflecting day time heating, or water may be slightly heated in the subsurface, despite the permafrost environment, perhaps due to exothermic pyrite oxidation at depth. More information is needed to confirm this hypothesis. Gypsum is most often found at sites with colder temperatures (at the base of the 50 cm core and in pits dug along transects), but otherwise mineralogy trends seem to be independent from temperature. Conductivity trends are subtle, but generally correspond with temperature trends. GD conductivity values range from 0.01 mS/cm (roughly that of very pure water, perhaps snowmelt) to 10.3 mS/cm (roughly one third that of seawater).

5.1.3. Implications for life

Temperature, pH, and conductivity ranges are all within acceptable limits for harbouring life during the summer; however, winter air temperatures are below 0 °C, and

ACCEPTED MANUSCRIPT

can be as low as -52 °C (Table 1). It is expected that the GD system freezes each winter, unless pyrite oxidation in the subsurface warms waters sufficiently to maintain perennial flow through the system, but we currently do not have sufficient data to confirm or refute this.

Visual observations of microbial filament and diatom communities by the field team, and phospholipid fatty acid analyses confirm that the GD is capable of supporting life for at least part of the year. Preliminary evidence indicates the widespread habitability of the GD by sulfate reducing bacteria (SRB) and a variety of other microbial organisms. Mineral by-products of SRB's were not observed, but could exist in abundances too small to be observed with XRD, or in an amorphous form of FeS, which would be undetectable by XRD. Sulfide levels are very high in water samples from seep sites. The slow streams of small bubbles noted at seeps were present in such small amounts that we could not collect them in the field, but these could be H_2S bubbles. Bubbles are likely not methane, based on composition of samples from the marsh surrounding GD. Regardless of bubble chemistry the high levels of sulfide at seeps could be a product of SRB in anoxic sediments in the subsurface. We do not yet have data to confirm this hypothesis, but it is the subject of ongoing work. Finally, although biochemical oxidation of pyrite is suspected to significantly accelerate reactions in the subsurface beneath the GD (van Everdingen et al., 1985), it is not a required mechanism for pyrite dissolution, either on Earth or Mars.

5.2. Mineralogy trends

ACCEPTED MANUSCRIPT

627 *5.2.1. Jarosite and natrojarosite*

628

629 Both jarosite ($KFe^{3+}_3(SO_4)_2(OH)_6$) and natrojarosite ($NaFe^{3+}_3(SO_4)_2(OH)_6$) have
630 been identified in varying proportions within most samples, as well as hydronium jarosite
631 ($(H_3O)Fe^{3+}_3(SO_4)_2(OH)_6$) in some samples. This is not unexpected, as the alunite
632 supergroup of minerals, including Na, K, and H_3O jarosite, show extensive solid solution
633 (e.g., Basciano and Peterson, 2007; Brophy and Sheridan, 1965). It was originally
634 reported that the GD contained natrojarosite (Michel, 1977), and subsequently reported
635 that the GD was composed primarily of jarosite (Michel and van Everdingen, 1987), but
636 it is now clear that both forms of jarosite are present and have likely coexisted within the
637 deposit for at least several decades, as indicated by unchanging water chemistry results
638 from 1975 to present. Natrojarosite will only precipitate after potassium has been
639 depleted (van Breemen, 1973), and hydronium jarosite most commonly precipitates in
640 very acidic environments (Basciano and Peterson, 2007). Thus, hydronium jarosite is
641 expected and observed at most acidic seep sites, and natrojarosite is expected to form
642 after jarosite precipitation has used up K^+ in water, explaining why Na- and K- jarosite
643 are commonly found together. This also explains why ICP-ES results show nearly equal
644 amounts of Na_2O and K_2O in most samples, yet waters are clearly enriched in Na^+
645 relative to K^+. Acidic sulfate soils in western and northern Canada are typically
646 comprised of natrojarosite in greater abundance than jarosite (Ross and Ivarson, 1981),
647 suggesting that overall, present-day groundwater in the region is likely richer in sodium
648 than potassium, as observed at the GD.

649

ACCEPTED MANUSCRIPT

ACCEPTED MANUSCRIPT

650 *5.2.2. Shale and detrital minerals*

651

652 Pyrite is expected yet has not been identified in the shale unit outcropping west of
653 the GD. This shale outcrop is at surface and highly weathered, therefore, it is not
654 surprising that no fresh sulfides were seen in that outcrop exposure. It does not mean that
655 no sulfides exist in the unit as a whole and at depth. It is presumed that pyrite has been
656 altered to jarosite here by a process similar to the one in the subsurface beneath the GD.
657 Along transects outward from the margins of the GD quartz, feldspar, mica, rutile, and
658 clays are all found in greater abundances than within the GD. Throughout the site
659 samples containing quartz almost always contain plagioclase, rutile, and phyllosilicates.
660 This combination suggests that quartz crystals are more likely detrital than authigenic. It
661 is thus assumed that these minerals are from the underlying shale or glacial till and have
662 made their way up through the GD by frost action (heaving). This process forms mud
663 boils in extreme cases, which would also disrupt any evidence of layering in the GD.

664

665 *5.3. Spatial trends*

666

667 *5.3.1. Trends at surface*

668

669 The mineralogy results presented here for GD crust samples differ from the
670 results presented by Michel and van Everdingen (1987). These authors reported that crust
671 samples collected in 1975 consisted of 56% goethite, 27% silicates, 9% jarosite, and 8%
672 gypsum. In samples from the present study, amounts of goethite are not noticeably larger

ACCEPTED MANUSCRIPT

673 in these samples than in many of the ochre samples, nor are jarosite amounts noticeably
674 smaller, and gypsum is not observed. Crust samples observed in this study were generally
675 enriched in sodium relative to wet ochre samples. Only one pH measurement, of 2.9, was
676 reported in 1975, which is consistent with present-day pH at seep sites. Thus, one
677 possible explanation is that the 1975 crust samples were collected at locations with higher
678 pH than 2008 sample sites. Higher pH could have led to stabilization of goethite and
679 gypsum, and dissolution of jarosite (Zolotov and Shock, 2005). Alternatively, there could
680 have been a higher water to rock ratio in the past, which would have caused a conversion
681 of jarosite to goethite (Zolotov and Shock, 2005). However, August 1st to mid September
682 1975 had about 50 mm of rain while the same period in 2008 saw approximately 90 mm
683 of rain for Norman Wells (Environment Canada, 2010a), so precipitation argues against
684 this hypothesis. A third possibility is that the differences may simply be a reflection of
685 the small number of samples collected. Differences are most likely due to a combination
686 of factors: the 2008 samples were taken at slightly greater depths, and from locations that
687 were probably closer to seeps. Thus pH was lower and jarosite more stable in the 2008
688 crust samples than the original samples.
689
690 *5.3.2. Trends with depth*
691
692 Caution must be exercised in determining trends with depth, as only one core
693 sample was taken. With this in mind, we note that concentrations of goethite, gypsum,
694 and hematite increase with depth, with the relative amount of jarosite correspondingly
695 decreasing with depth. According to the pH-Eh-hydration path for Fe-sulfide weathering,

ACCEPTED MANUSCRIPT

there is a natural progression towards goethite and hematite (Jerz and Rimstidt, 2003). Increased pH also stabilizes gypsum (Zolotov and Shock, 2005). Thus, it might be assumed that goethite and gypsum abundances would increase with weathering of exposed surfaces and, therefore, increase at the surface and decrease with depth, as was observed in crusts by Michel and van Everdingen (1987). Likewise, if hematite were to form through dehydration of goethite, for example through desiccation of the GD due to an especially dry summer, or heating (although heating sufficient to drive off water is unlikely at the GD), it would be expected to appear in areas of decreased saturation, more likely to occur at the surface than at depth. We hypothesize that the GD is building layers upwards, as seeps penetrate up through older materials to the surface to continuously deposit freshly precipitated material on top. The vertical trends observed in mineral concentration at this single site may be the result of past surface or shallow subsurface alteration or dehydration of jarosite phases that were previously precipitated on the surface and have been buried.

Despite our hypothesis that the GD is precipitating jarosite upward in layers, visual evidence of layering has not been noted. It is also unclear how material is currently being deposited in drier portions of the GD, if layers are built up from seeps. Channels account for some lateral transportation of material, but at least half of the GD surface is currently relatively dry and untouched by channels. The GD could be covered by water during the spring melt, which may provide a mechanism for sediment transport. Alternatively, seep locations may have changed over the years, accounting for this deposition.

ACCEPTED MANUSCRIPT

719 *5.3.3. Trends radially outward from GD*

720

721 Transect samples were analysed to determine whether or not jarosite is present
722 beyond the main exposed deposit. Assuming jarosite layers were deposited on the surface
723 as opposed to at depth, the presence of jarositic soils extending beneath vegetation and
724 outward from the main deposit may indicate the system has been active for at least as
725 long as it took the oldest trees to grow. However, it is also possible that jarosite was
726 deposited beneath surrounding vegetation, including trees, although there is no visual
727 evidence that plant health has been affected adversely. The GD appears to be situated on
728 top of a glacial till that would have been exposed to weathering for a period of time after
729 deglaciation and prior to the formation of the GD. Constraining the age of the deposit is
730 the subject of ongoing work

731 Samples taken from transects were found to have a similar composition to the
732 samples within the main deposit, but in differing proportions. More gypsum and less
733 jarosite and natrojarosite are noted with increasing distance from the exposed GD,
734 suggesting that gypsum is preferentially precipitated over jarosite, or that jarosite is
735 altering and contributing sulfate to gypsum deposition. In addition, two transect samples
736 were analyzed for oxides. Although it is difficult to draw conclusions from only two
737 samples, a few trends have been observed. K_2O is more abundant in the two transect
738 samples than Na_2O, suggesting less Na_2O is present outside of the exposed deposit than
739 within the deposit, and perhaps the chemistry of the GD has changed over time. MgO and
740 CaO are also enriched in transect samples relative to the GD, in addition to SiO_2, Al_2O_3,
741 and TiO_2 (likely from detrital minerals). Overall, there is less Fe_2O_3, Na_2O, and K_2O in

ACCEPTED MANUSCRIPT

transects; this may simply be in response to the increased concentrations of SiO_2, Al_2O_3, and TiO_2.

The increase in pH along transects suggests that seeps are not currently active outside of the main deposit, except in a few isolated cases. Thus, the acidic conditions characteristic of the GD site are isolated from the surrounding environment. Beyond a radius of approximately 70 m from the GD, water pH, temperature, and soil mineralogy are not influenced by acidic groundwater, and no other jarosite patches have been observed in the surrounding area. This may suggest that martian acid aqueous systems could also have been isolated from surrounding neutral or alkaline systems, and thus may have persisted penecontemporaneously with them, rather than dominating the entire surface of Mars for a period of time. If this were the case, acid aqueous systems, although spatially constrained, may not have been temporally constrained.

5.4. Temporal trends

Recent aerial surveys of the GD have revealed few discernible physical changes in the deposit since it was last surveyed over 30 years ago. It seems that the deposit has increased in size, as dimensions were measured at 126 × 46.5 m in the 1970s, and dimensions from this study were measured as 140 m × 50 m. Water chemistry data reported in 1987 (Michel and van Everdingen) is similar to water chemistry presented here, suggesting that the chemistry of the system has been relatively stable over the past few decades. One notable difference was the smaller quantity of evaporitic salt crusts deposited around the edges of the deposit and on leaves of plants, than previously

ACCEPTED MANUSCRIPT

765 observed. Michel and van Everdingen (1987) originally observed these encrustations on
766 September 15th, 1975, and suggested that they form through the evapotranspiration of
767 saline groundwater. Perhaps fewer were witnessed on September 13th and 14th, 2008
768 because of dissolution of evaporitic crusts by recent rainfall. Air temperature and
769 precipitation records from the Environment Canada (2010a) database for Norman Wells
770 indicate double the amount of rain in 2008 compared to 1975 for the 45 day period prior
771 to the site visits, and that temperatures in 2008 were cooler by 5 °C.
772
773 *5.5. Implications for Mars*
774
775 *5.5.1. Spectral identification of jarosite from orbit*
776
777 Spectrally and mineralogically the Golden Deposit is dominated by jarosite and
778 natrojarosite. The spectrum we produced by a linear mixture of spectra of the 21 surficial
779 samples is analogous to a spectrum that could be acquired by an orbital instrument flying
780 over a jarositic deposit on the surface of Mars (Fig. 6), and thus it can be used as ground
781 truth for the Compact Reconnaissance Imaging Spectrometer for Mars (CRISM). This
782 works particularly well when sulfate minerals are dominated by jarosite, due to the
783 stability of jarosite under martian conditions. According to Cloutis et al. (2008), most
784 terrestrial sulfates experience some shift in absorption features when exposed to martian
785 atmospheric conditions for days to weeks; however, jarosite does not change owing to its
786 thermodynamic stability on Mars (Navrotsky et al., 2005). Thus, the GD linear mixture
787 spectrum can be directly compared to smoothed CRISM spectral data published by

ACCEPTED MANUSCRIPT

ACCEPTED MANUSCRIPT

Farrand et al. (2009) from an ovoid patch in the Mawrth Vallis region of Mars (Fig. 7), interpreted to be dominated by the presence of jarosite or natrojarosite. Both show jarosite absorption features at 2.26 and 2.46 μm, and other minerals are masked. As has been learned from discoveries by the Mars Exploration Rovers, spectra with the relative coarseness of orbital imagery are only useful for identifying the major mineralogy and drawing coarse-scale conclusions. This especially applies when spectra are obtained from jarosite-dominated locations. Therefore, spectral analysis has limitations as a remote sensing technique, and ground-truthing is very important to gain a detailed understanding of a jarositic site of this nature. For regions of Mars where the only current mineralogical data set is remote spectra from orbit (most of the planet), we are likely missing many other intermingled minor mineralogical components, which may significantly help to explain geological, hydrological, and potentially biological colonization of any given area.

5.5.2. Comparison to jarosite on Mars

The basic ingredients needed to create a surficial jarosite patch on Mars similar to the Golden Deposit are: 1. Fe-sulfides at depth, 2. groundwater circulation and upwelling, and 3. arid, oxidizing surface conditions. There is evidence for all three ingredients in or on Mars at a planetary scale. Although permafrost does not seem to be a required ingredient it does not inhibit surficial jarosite precipitation. Meteorite evidence demonstrates the occurrence of Fe-sulfides in the martian subsurface (E.g., McSween and Treiman, 1998; Treiman, 2003). There is abundant evidence for the past presence of surface water on Mars, particularly during the Noachian, and it is likely that some form

ACCEPTED MANUSCRIPT

811 of groundwater circulation occurred in the past, and may persist to the present (Bibring et
812 al., 2006; Squyres et al., 2004b). Finally, oxidizing conditions prevail on the surface of
813 Mars.

814 The GD represents an intriguing analogue to past aqueous processes and
815 habitability at both Meridiani Planum and Mawrth Vallis, as mineralogy, groundwater,
816 permafrost conditions, and arid conditions at the time of deposition are potentially
817 comparable. Mineralogy of the GD is very similar to that of Meridiani Planum, as
818 determined using data from the Mars Exploration Rover Opportunity. Meridiani Planum
819 features jarosite plus Mg- and Ca-sulfates, in addition to hematite spherules (Christensen
820 et al., 2004; Klingelhofer et al., 2004; Squyres et al., 2004b; Squyres et al., 2006), while
821 GD features jarosite plus Ca-sulfates and iron-oxide deposits. The 3 × 5 km ovoid
822 jarositic deposit at Mawrth Vallis was discovered using data from the Mars
823 Reconnaissance Orbiter (MRO) Compact Reconnaissance Imaging Spectrometer for
824 Mars (CRISM) hyperspectral imager. It sits within a depression in layered terrains and
825 has surficial polygonal fracture patterns (Farrand et al., 2009). This ovoid patch features
826 thin ferric oxide coatings, which may be goethite on jarosite. GD is similar in terms of
827 mineralogy, as well as scale and appearance to the jarosite deposit at Mawrth Vallis.
828 Observations of sulfate-rich sedimentary rocks from microscopic to orbital scales suggest
829 that ancient Meridiani Planum once had abundant acidic, sulfate-rich groundwater, arid
830 and oxidizing surface conditions, and occasional liquid flow on the surface, followed by a
831 period of evaporation and desiccation (Squyres et al., 2004b). The same groundwater and
832 environmental conditions could be inferred for Mawrth Vallis; however, less is currently
833 known about this site, as observations are restricted to orbital data. While the origin of

ACCEPTED MANUSCRIPT

834 the Fe/Mg-phyllosilicate-bearing unit underlying the ovoid jarosite patch at Mawrth
835 Vallis cannot be determined from orbital data, it is likely sedimentary in nature
836 (Michalski et al., 2010) . Thus, it may be directly comparable to the sedimentary bedrock
837 beneath the GD, which once contained pyrite (although, sedimentary rocks are not a
838 requirement for the occurrence of similar jarosite deposition mechanisms). The
839 possibility of Fe-sulfides at depth at Mawrth Vallis could suggest a similar jarosite
840 formation mechanism through Fe-sulfide oxidation by upwelling acidic groundwater and
841 precipitation at the surface.

842 If the Mawrth Vallis jarosite patch was formed by upwelling of acidic
843 groundwater and subsequent precipitation of sulfates, this could provide more incentive
844 to explore Mawrth Vallis. This region could offer even more than previously thought in
845 terms of potential evidence of aqueous paleoenvironments and past habitability. It has
846 been suggested that Mawrth Vallis is an ideal place to search for organics preserved in
847 phyllosilicates during Mars' earlier alkaline aqueous period (Michalski et al., 2010), and
848 that sulfate deposits could provide information about a later acidic saline aqueous period
849 on Mars (Bibring et al., 2006). Regardless of the temporal relationship between the
850 Mawrth Vallis jarosite patch and the surrounding phyllosilicates, we suggest that sulfate
851 deposits at Mawrth Vallis should be a high priority target in the search for preserved
852 organics. The GD jarosite is similar in many ways to jarosite at Rio Tinto, and thus
853 analogies can be drawn between these two terrestrial jarosite deposits, and those already
854 reported (and yet to be discovered) at Mawrth Vallis. The Rio Tinto River has been a
855 natural, active acid rock drainage site for more than 2 million years, and has supported
856 and preserved a diverse microbial community for the duration of its existence (Amaral

ACCEPTED MANUSCRIPT

Zettler et al. 2002; Sabater et al. 2003; Aguilera et al. 2006). Rock and sediment samples from Rio Tinto, including jarosite, goethite, and hematite, ranging from present day to 2 Ma, have been shown by Preston et al. (2011) to preserve biomolecules and morphological evidence of life. The morphology of microbial cells has been preserved in these samples, and confirmed to contain organic material through FTIR spectroscopy. The preservation potential of microorganisms and organic molecules within iron-rich sedimentary rocks and sulfates has been discussed by Sumner (2004) and references therein.

Experiments by Ohmoto and Lasaga (1982) imply that sulfates such as jarosite have the potential to preserve organics over geologic time scales, as although reactions between sulfates and organic compounds are possible at very low pH, these reactions are not likely to lead to the decay of organics in the absence of a biological sulfate reduction metabolism. Furthermore, most microorganisms are known to possess lytic enzymes, also known as autolysins that are capable of degrading their cell walls (Beveridge, 1981). Autolytic activity is inhibited by iron, as metals bound by bacterial walls maintain the constituent polymers of these cellular structures in a conformation unfavourable to autolysin attack (Van Heijenoort et al., 1983). Therefore, the scavenging of iron from the environment by bacterial cell envelopes can prevent or limit cell degradation and form an integral part in a series of events leading to the fossilization of microorganisms (Ferris et al., 1988). Therefore, environments on Mars such as Meridiani Planum and Mawrth Vallis, which have similarities to the GD and Rio Tinto deposits, could have supported and preserved evidence of life.

ACCEPTED MANUSCRIPT

In addition, the GD demonstrates that geochemical heterogeneity at the sub-metre scales can exist at a seemingly homogeneous deposit (as observed by orbital spectroscopy or aerial photos), and indicates that there is likely much yet to be discovered at similar sites on Mars via robotic or human surface missions. Regardless of the jarosite deposition mechanism, the fact that Mawrth Vallis was considered as a possible landing site, and may be considered for future missions, makes the GD especially important as an analogous test bed for hypotheses. GD could also be used for ground truthing data that may one day be returned from sulfate deposits at Mawrth Vallis.

6. Conclusions

Cold, acidic springs represent a good depositional analogue to past aqueous environments on Mars. Sedimentary deposits found in Meridiani Planum and composed mainly of Ca-, Mg- and Fe-sulfates and iron oxides are thought to have formed from the upwelling and evaporation or freezing/sublimation of surface or near surface waters. Similar mineral assemblages have been found on other parts of the planet, including Mawrth Vallis, suggesting that cold, acidic groundwater could have influenced the geochemistry of surface water for extended periods of time (Fairén et al., 2004), at least in isolated locations. Although permafrost was not likely required for the GD to form, this site demonstrates that conditions on Mars did not need to be significantly warmer or wetter than today for jarosite deposition. Low water pH would have constrained the type of mineral deposits that could have precipitated and also the habitability of surface waters.

ACCEPTED MANUSCRIPT

ACCEPTED MANUSCRIPT

The jarositic, cold seep emplaced Golden Deposit is similar to Meridiani Planum and Mawrth Vallis, Mars, in terms of chemistry, mineralogy, permafrost environment at the time of deposition, and to some degree also in terms of scale, albedo, surface texture, and geomorphology. The mineralogy and geochemistry of the GD, as determined by XRD and ICP-ES, have proven to be much more complex than indicated by spectral analysis alone. Therefore mineral assemblages containing jarosite on Mars may be more complex than the current spectral data leads us to believe. Despite low pH and cool temperatures, the GD is hospitable to microbial life. If jarosite deposits on Mars were emplaced by a similar groundwater upwelling mechanism, under similar pH and temperature conditions, they may also have supported life, and may even contain evidence of past life preserved within the sediments. Therefore, the GD presents a new possible analogue site for studying jarosite deposition on Mars, and is the only documented site on Earth featuring spectrally pure jarosite at an orbital scale in a permafrost setting. It is of special interest, as Mawrth Vallis or Meridiani Planum may be considered as potential landing sites for future missions to look for signs of life on Mars.

Acknowledgements

Roberta Flemming is thanked for guidance with mineral identification and the use of the EVA software, and Kim Law is thanked for guidance with the use of the XRD. Nicola Barry is thanked for assistance in the lab. We also wish to thank two anonymous reviewers for their helpful feedback. This study was supported by grants from the Canadian Space Agency (CSA) Canadian Analogue Research Network (CARN) and the Natural Science and Engineering Research Council of Canada (NSERC) to GRO.

ACCEPTED MANUSCRIPT

925 **REFERENCES**

926

927 Aguilera, A., Manrubia, S.C., Gomez, F., Rodriguez, N., Amils, R., 2006. Eukaryotic
928 community distribution and its relationship to water physicochemical parameters
929 in an extreme acidic environment, Rio Tinto (southwestern Spain). Applied and
930 Environmental Microbiology 72, 5325-5330.
931 Amaral-Zettler, L.A., Gómez, F., Zettler, E., Keenan, B.G., Amils, R., Sogin, M.L., 2002.
932 Eukaryotic diversity in Spain's river of fire. Nature 417, 137.
933 Amils, R., et al., 2007. Extreme environments as Mars terrestrial analogs: The Rio Tinto
934 case. Planetary and Space Science 55, 370-381.
935 Andrews-Hanna, J.C., Zuber, M.T., Arvidson, R.E and S. M. Wiseman., 2010. Early
936 Mars hydrology: Meridiani playa deposits and the sedimentary record of Arabia
937 Terra. J. Geophysical Research 115, 1-22.
938 Baldridge, A.M., et al., 2009. Contemporaneous deposition of phyllosilicates and sulfates:
939 Using Australian acidic saline lake deposits to describe geochemical variability on
940 Mars. Geophysical Research Letters 36, L19201.
941 Basciano, L.C., Peterson, R.C., 2007. Jarosite hydronium jarosite solid-solution series
942 with full iron site occupancy: Mineralogy and crystal chemistry. American
943 Mineralogist 92, 1464-1473.
944 Benison, K.C., and LaClair, D.A., 2003. Modern and Ancient Extremely Acid Saline
945 Deposits: Terrestrial Analogs for Martian Environments? Astrobiology 3, 609-618.
946 doi:10.1089/153110703322610690.

ACCEPTED MANUSCRIPT

ACCEPTED MANUSCRIPT

947 Beveridge, T.J., 1981. Ultrastructure, chemistry, and function of the bacterial wall.
948 International Review of Cytology 72, 229-317.
949 Bibring, J.-P., et al., 2006. Global mineralogical and aqueous Mars history derived from
950 OMEGA/Mars Express data. Science 312, 400-404.
951 Bibring, J.P., et al., 2007. Coupled ferric oxides and sulfates on the martian surface.
952 Science 317, 1206-1210.
953 Bonaccorsi, R., Stoker, C.R., 2008. Science results from a Mars drilling simulation (Río
954 Tinto, Spain) and ground truth for remote science observations. Astrobiology 8,
955 967-985.
956 Brophy, G.P., Sheridan, M.F., 1965. Sulfate studies IV: The jarosite-natrojarosite-
957 hydronium jarosite solid solution series. American Mineralogist 50, 1595-1607.
958 Buckby, T., Black, S., Coleman, M.L., Hodson, M.E., 2003. Fe-sulphate-rich evaporative
959 mineral precipitates from the Rio Tinto, southwest Spain. Mineralogical Magazine
960 67, 263-278.
961 Carr, M.H., Head, J.W., III, 2003. Oceans on Mars: An assessment of the observational
962 evidence and possible fate. J. Geophys. Res. 108, 5042.
963 Carr, M.H., Schaber, G.G., 1977. Martian permafrost features. Journal of Geophysical
964 Research 82, 4039–4054.
965 Chevrier, V., Poulet, F., Bibring, J.-P., 2007. Early geochemical environment of Mars as
966 determined from thermodynamics of phyllosilicates. Nature 448, 60-63.
967 Christensen, P.R., 2008. The compositional diversity and physical properties mapped
968 from the Mars Odyssey Thermal Emission Imaging System, In: Bell III, J.F. (Ed.),

ACCEPTED MANUSCRIPT

969 The Martian Surface: Composition, Mineralogy and Physical Properties.
970 Cambridge University Press, New York, p. 652.
971 Christensen, P.R., et al., 2004. Mineralogy at Meridiani Planum from the Mini-TES
972 Experiment on the Opportunity Rover. Science 306, 1733-1739.
973 Cloutis, E., Craig, M., Kaletzke, L., McCormack, K., Stewart, L., 2006a. HOSERLab: A
974 new Planetary Spectrophotometer Facility, 37th Lunar and Planetary Science
975 Conference, Abstract #2121.
976 Cloutis, E., et al., 2008. Spectral reflectance properties of minerals exposed to simulated
977 Mars surface conditions. Icarus 195, 140-168.
978 Cloutis, E., et al., 2006b. Detection and discrimination of sulfate minerals using
979 reflectance spectroscopy. Icarus 184, 121-157.
980 Ehlmann, B.L., et al., 2011. Subsurface water and clay mineral formation during the early
981 history of Mars. Nature 479, 53-60.
982 Fairén, A.G., 2010. A cold and wet Mars. Icarus 208, 165-175.
983 Fairén, A.G., Davila, A.F., Gago-Duport, L., Amils, R., McKay, C.P., 2009. Stability
984 against freezing of aqueous solutions on early Mars. Nature 459, 401-404.
985 Fairén, A.G., et al., 2011. Cold glacial oceans would have inhibited phyllosilicate
986 sedimentation on early Mars. Nature Geosci 4, 667-670.
987 Fairén, A.G., Fernandez-Remolar, D., Dohm, J.M., Baker, V.R., Amils, R., 2004.
988 Inhibition of carbonate synthesis in acidic oceans on early Mars. Nature 431, 423-
989 426.

ACCEPTED MANUSCRIPT

ACCEPTED MANUSCRIPT

990 Farrand, W.H., Glotch, T.D., Rice Jr, J.W., Hurowitz, J.A., Swayze, G.A., 2009.
991 Discovery of jarosite within the Mawrth Vallis region of Mars: Implications for the
992 geologic history of the region. Icarus 204, 478-488.
993 Fernández-Remolar, D.C., Morris, R.V., Gruener, J.E., Amils, R., Knoll, A.H., 2005. The
994 Río Tinto Basin, Spain: Mineralogy, sedimentary geobiology, and implications for
995 interpretation of outcrop rocks at Meridiani Planum, Mars. Earth and Planetary
996 Science Letters 240, 149-167.
997 Ferris, F.G., Fyfe, W.S., Beveridge, T.J., 1988. Metallic ion binding by Bacillus subtilis:
998 Implications for the fossilization of microorganisms. Geology 16, 149-152.
999 Harris, S.A., et al., 1988. Glossary of permafrost & related ground-ice terms, In:
1000 Subcommittee, P. (Ed.), Assoc. Comm. on Geotechnical Research Technical
1001 Memorandum NRC, Ottawa, p. 156.
1002 Hudson-Edwards, K.A., Schell, C., Macklin, M.G., 1999. Mineralogy and geochemistry
1003 of alluvium contaminated by metal mining in the Rio Tinto area, southwest Spain.
1004 Applied Geochemistry 14, 1015-1030.
1005 Hurowitz, J.A., Fischer, W.W., Tosca, N.J., Milliken, R.E., 2010. Origin of acidic surface
1006 waters and the evolution of atmospheric chemistry on early Mars. Nature Geosci 3,
1007 323-326.
1008 Jerz, J.K., Rimstidt, J.D., 2003. Efflorescent iron sulfate minerals: Paragenesis, relative
1009 stability, and environmental impact. American Mineralogist 88, 1919-1932.
1010 Johnson, S.S., Mischna, M.A., Grove, T.L., Zuber, M.T., 2008. Sulfur-induced
1011 greenhouse warming on early Mars. Journal of Geophysical Research: Planets 113,
1012 1-15.

ACCEPTED MANUSCRIPT

ACCEPTED MANUSCRIPT

1013 Klingelhofer, G., et al., 2004. Jarosite and hematite at Meridiani Planum from
1014 Opportunity's Mossbauer spectrometer. Science 306, 1740-1745.
1015 Kretz, R., 1983. Symbols for rock-forming minerals. American Mineralogist 68, 277-279.
1016 Lacelle, D., Léveillé, R., 2010. Acid drainage generation and associated Ca-Fe-SO4
1017 minerals in a periglacial environment, Eagle Plains, Northern Yukon, Canada: A
1018 potential analogue for low-temperature sulfate formation on Mars. Planetary and
1019 Space Science 58, 509-521.
1020 McSween, H.Y., Treiman, A.H., 1998. Martian Meteorites. Mineralogical Society of
1021 America, Washington, DC.Mellon, M.T., Phillips, R.J., 2001. Recent gullies on
1022 Mars and the source of liquid water. J. Geophys. Res. 106, 23165-23179.
1023 Michalski, J.R., et al., 2010. The Mawrth Vallis region of Mars: A potential landing site
1024 for the Mars Science Laboratory (MSL) mission. Astrobiology 10, 687-703.
1025 Michalski, J.R., Niles, P.B., 2011. Formation of jarosite in the Mawrth Vallis region of
1026 Mars by weathering within paleo-ice deposits, 42nd Lunar and Planetary Science
1027 Conference, Abstract #1926.
1028 Michel, F.A., 1977. Hydrogeologic studies of springs in the Central Mackenzie Valley,
1029 North West Territories, Canada. University of Waterloo, M.Sc. thesis,Waterloo
1030 Ontario.
1031 Michel, F.A., van Everdingen, R.O., 1987. Formation of a jarosite deposit on Cretaceous
1032 shales in the Fort Norman area, Northwest Territories. Canadian Mineralogist 25,
1033 221-226.
1034 Mitrofanov, I.G., et al., 2003. CO_2 snow depth and subsurface water-ice abundance in the
1035 northern hemisphere of Mars. Science 300, 2081-2084.

ACCEPTED MANUSCRIPT

ACCEPTED MANUSCRIPT

1036 Navrotsky, A., Forray, F., Drouet, C., 2005. Jarosite stability on Mars. Icarus 176, 250-
1037 253.
1038 Ohmoto, H., Lasaga, A.C., 1982. Kinetics of reactions between aqueous sulfates and
1039 sulfides in hydrothermal systems. Geochimica et Cosmochimica Acta 46, 1727-
1040 1745.
1041 Papike, J.J., Karner, J.M., Spilde, M.N., Shearer, C.K., 2006. Terrestrial analogs of
1042 martian sulfates: Major and minor element systematics of alunite-jarosite from
1043 Goldfield, Nevada. American Mineralogist 91, 1197-1200.
1044 Parker, T.J., Gorsline, D.S., Saunders, R.S., Pieri, D.C., Schneeberger, D.M., 1993.
1045 Coastal Geomorphology of the Martian Northern Plains. J. Geophys. Res. 98,
1046 11061-11078.
1047 Phillips, R.J., et al., 2008. Mars north polar deposits: Stratigraphy, age, and geodynamical
1048 response. Science 320, 1182-1185.
1049 Pollack, J.B., Kasting, J.F., Richardson, S.M., Poliakoff, K., 1987. The case for a wet,
1050 warm climate on early Mars. Icarus 71, 203-224.
1051 Preston, L.J., Shuster, J., Fernández-Remolar, D., Banerjee, N.R., Osinski, G.R., Southam,
1052 G., 2011. The preservation and degradation of filamentous bacteria and
1053 biomolecules in iron oxide deposits from Rio Tinto, Spain. Geobiology 9, 233-
1054 249.Ross, G.J., Ivarson, K.C., 1981. The occurrence of basic ferric sulphates in
1055 some Canadian soils. Canadian Journal of Earth Sciences 61, 99-107.
1056 Rossman, G.R., 1976. Spectroscopic and magnetic studies of ferric iron hydroxy sulfates:
1057 the series $Fe(OH)SO_4 \bullet nH_2O$ and the jarosites. American Mineralogist 61, 398-404.

ACCEPTED MANUSCRIPT

ACCEPTED MANUSCRIPT

1058 Rühland, K., Smol, J.P., 1998. Limnological characteristics of 70 lakes spanning Arctic
1059 treeline from Coronation Gulf to Great Slave Lake in the central Northwest
1060 Territories, Canada. International Review of Hydrobiology 83, 183-203.
1061 Sabater, S., et al., 2003. Structure and function of benthic algal communities in an
1062 extremely acid river. Journal of Phycology 39, 481-489.
1063 Sherman, D.M., and Waite, T.D., 1985. Electronic spectra of Fe^{3+} oxides and oxide
1064 hydroxides in the near IR to near UV. American Mineralogist 70, 1262-1269.
1065 Smith, P.H., et al., 2009. H2O at the Phoenix landing site. Science 325 58-61.
1066 Spanovich, N., Smith, M.D., Smith, P.H., Wolff, M.J., Christensen, P.R., Squyres, S.W.,
1067 2006. Surface and near-surface atmospheric temperatures for the Mars Exploration
1068 Rover landing sites. Icarus 180, 314-320.
1069 Squyres, S.W., et al., 2004a. The Opportunity Rover's Athena science investigation at
1070 Meridiani Planum, Mars. Science 306, 1698-1703.
1071 Squyres, S.W., et al., 2004b. In situ evidence for an ancient aqueous environment at
1072 Meridiani Planum, Mars. Science 306, 1709-1714.
1073 Squyres, S.W., et al., 2006. Two years at Meridiani Planum: Results from the
1074 Opportunity Rover. Science 313, 1403-1407.
1075 Sumner, D.Y., 2004. Poor preservation potential of organics in Meridiani Planum
1076 hematite-bearing sedimentary rocks. Journal of Geophysical Research 109, E12007.
1077 Treiman, A.H., 2003. Chemical compositions of martian basalts (shergottites): Some
1078 inferences on basalt formation, mantle metasomatism, and differentiation on Mars.
1079 Meteoritics & Planetary Science 38, 1849-1864.

ACCEPTED MANUSCRIPT

ACCEPTED MANUSCRIPT

1080 van Breemen, N., 1973. Soil forming processes in acid sulphate soils, In: Dost, H. (Ed.),
1081 Acid Sulphate soils. Institute for Land Reclaimation and Improvement Wageningen,
1082 the Netherlands, pp. 66–130.
1083 van Everdingen, R.O., Shakur, M.A., Michel, F.A., 1985. Oxygen- and sulfur- isotope
1084 geochemistry of acidic groundwater discharge in British Columbia, Yukon, and
1085 District of Mackenzie, Canada. Canadian Journal of Earth Sciences 22, 1689-1695.
1086 Van Heijenoort, J., Leduc, M., Van Heijenoort, Y., Kasra, R., 1983. Autolysis of
1087 Escherichia coli: Induction and control. Walter de Gryter and Co., Berlin, pp. 191-
1088 196.
1089 Varekamp, J.C., Pasternack, G.B., Rowe Jr, G.L., 2000. Volcanic lake systematics II.
1090 Chemical constraints. Journal of Volcanology and Geothermal Research 97, 161-
1091 179.
1092 Warner, T.T., 2004. Desert Meteorology. Cambridge University Press, New York, 597p.
1093 West, L., McGown, D.J., Onstott, T.C., Morris, R.V., Suchecki, P., Pratt, L.M., 2009.
1094 High Lake gossan deposit: An Arctic analogue for ancient Martian surficial
1095 processes? Planetary and Space Science 57, 1302-1311.
1096 Yorath, C.J., Cook, D.G., 1981. Cretaceous and Tertiary stratigraphy and paleogeography,
1097 northern interior plains, District of Mackenzie, Geological Survey of Canada,
1098 Ottawa, p. 76.
1099 Zolotov, M.Y., Shock, E.L., 2005. Formation of jarosite-bearing deposits through
1100 aqueous oxidation of pyrite at Meridiani Planum, Mars. Geophys. Res. Lett. 32,
1101 L21203.
1102

ACCEPTED MANUSCRIPT

WEB REFERENCES

Environment Canada, 2010a, The Weather Network Statistics: Norman Wells, NT, Canada. Last accessed January 27, 2011. http://www.theweathernetwork.com/statistics/summary/cl2202800

Environment Canada, 2010b, The Weather Network Statistics: Old Crow, YT, Canada. Last accessed January 27, 2011. http://www.theweathernetwork.com/statistics/CL2100800/cayt0012/

ACCEPTED MANUSCRIPT

ACCEPTED MANUSCRIPT

FIGURES

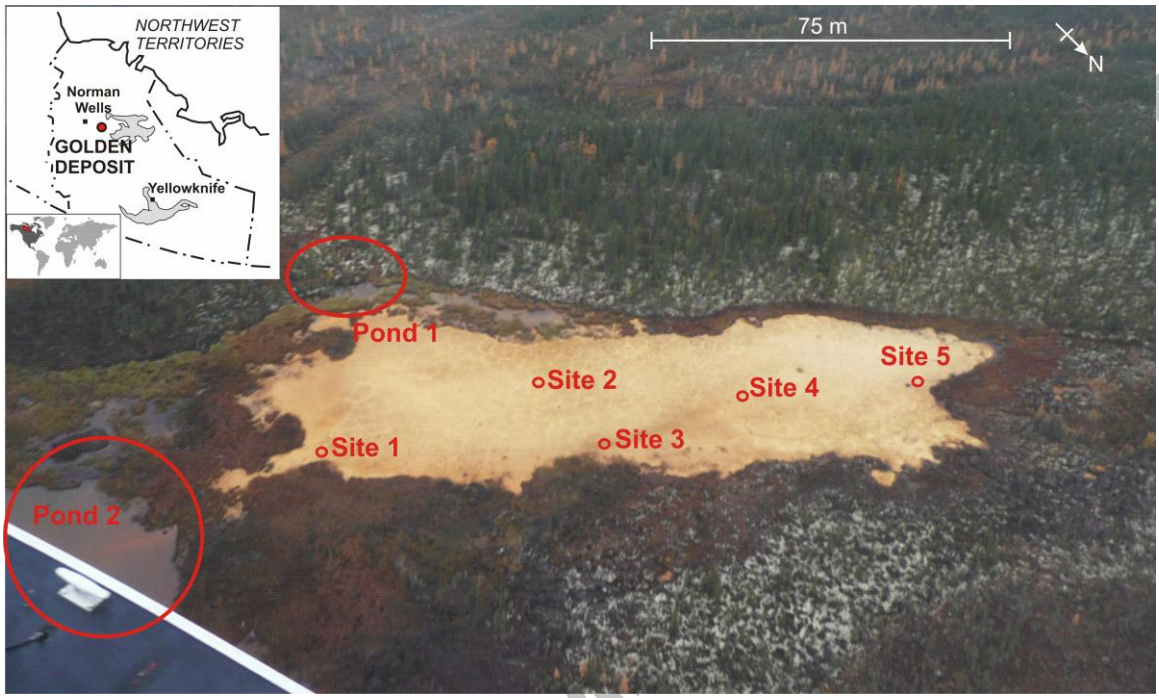

Fig. 1. Aerial photograph of the Golden Deposit, taken during September 2009. Note polygonal surface patterns, which look like fractures from this altitude. Inset map of Northwest Territories, Canada showing approximate location of the Golden Deposit, south east of Norman Wells, and world map showing location of Northwest Territories, Canada.

ACCEPTED MANUSCRIPT

ACCEPTED MANUSCRIPT

Fig. 2. Images of the Golden Deposit. A: Water flows through troughs surrounding 1 – 3 m polygonal "islands". Areas within polygonal islands are dry and sufficiently hard to stand on. B: Close-up view of a typical area within the GD; mud is composed primarily of various phases of jarosite, as well as some quartz and goethite, and other minor minerals. Crust samples were obtained from the surface, near polygon centres, and ochre samples were obtained from the surface and subsurface (cm's) usually closer to channels in polygon troughs. C: Push core sample from the surface to 50 cm depth. Note poorly sorted silt, and smaller amounts of sand and gravel. D: Example of a transect sample 20 m out from GD; jarosite mud exposed several cm's beneath organic overburden. E: Evaporitic salt crust sample scraped from vegetation and mud proximal to the GD. F: 60 cm deep trench dug into shale outcrop west of the GD; note zones of red (hematite, goethite, and other minerals) and yellow-ish orange (goethite, jarosite, and other minerals). G: Suspected microbial community forming streamer-style biofilaments in relatively fast-flowing water below scale bar. H: Terraces formed near streamers also suspected to support a microbial community. I: Examples of active seeps within the Golden Deposit, indicated by arrows. Seeps shown here range in diameter from 1 cm (right) to 6 cm (middle).

ACCEPTED MANUSCRIPT

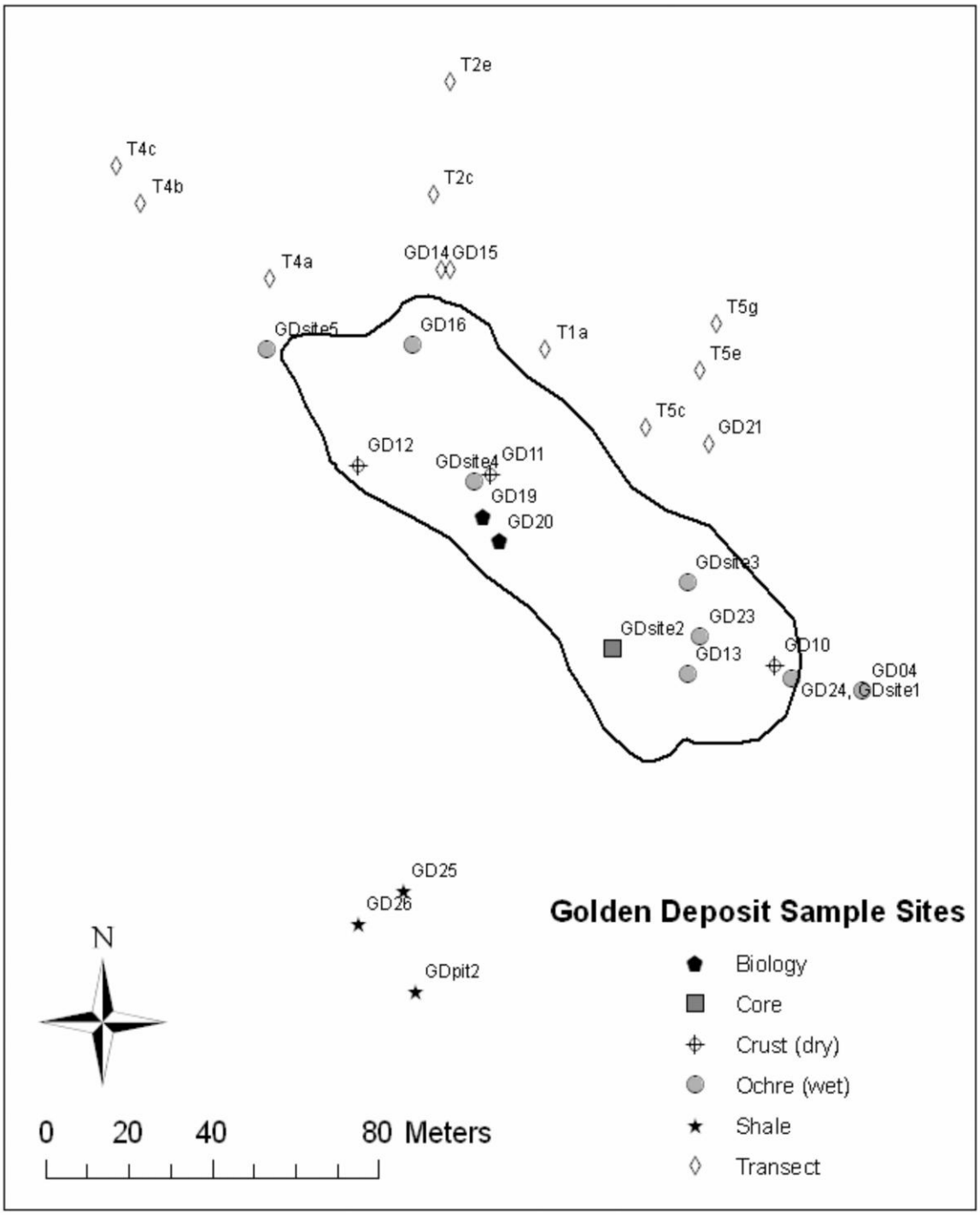

Fig. 3. Map of sample sites, including locations of terrace and biofilament samples (biology), 50 cm core site (pH = 2.78), dry surface samples (crust), wet surface samples (ochre), samples from a pit in the shale outcrop west of the deposit (shale), and samples from transects to the NW, N, and E of the GD.

1179

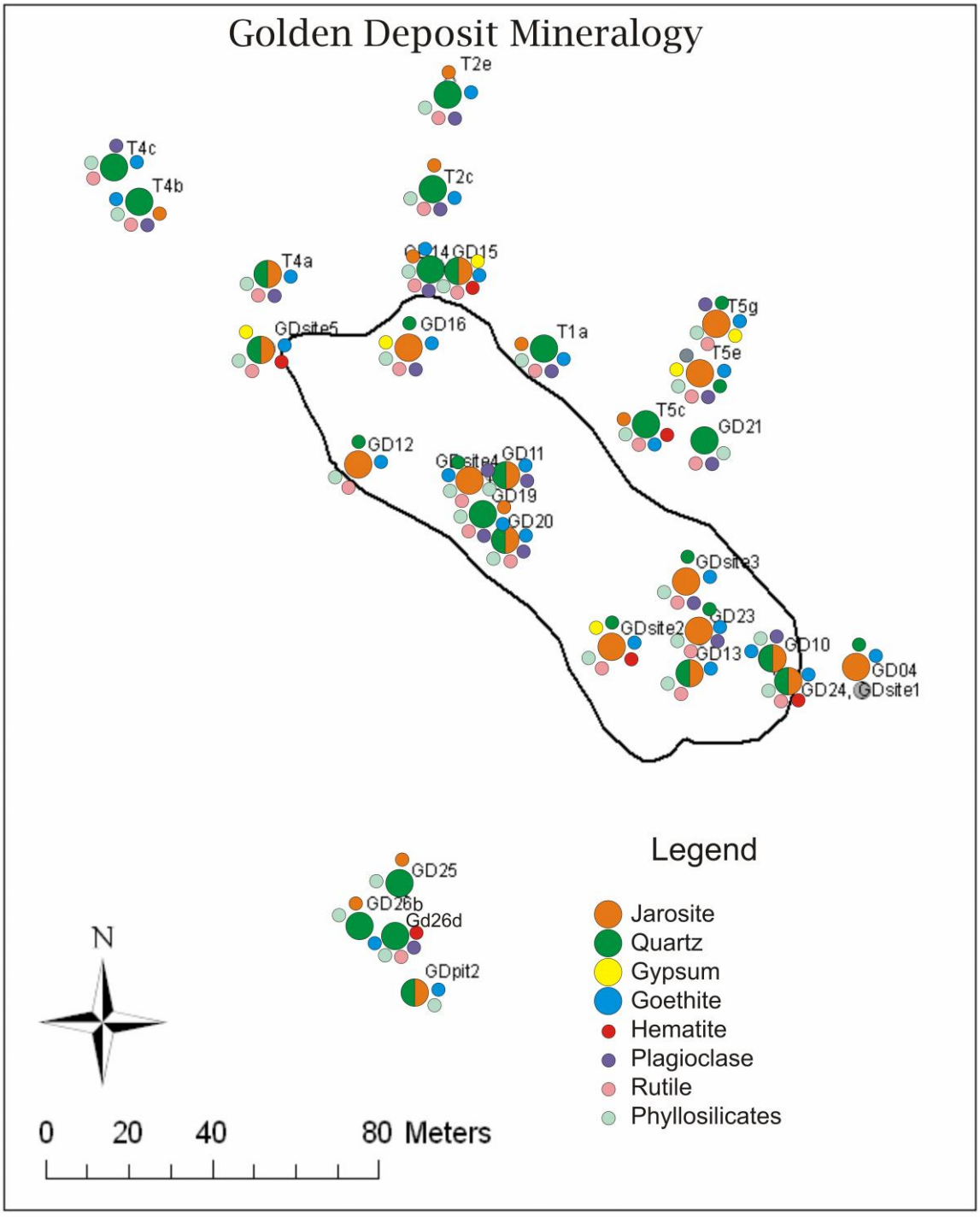

1180
1181

1182 **Fig. 4.** Mineralogy of samples as determined by XRD. All three forms of jarosite
1183 (natrojarosite ($NaFe^{3+}_3(SO_4)_2(OH)_6$), jarosite ($KFe^{3+}_3(SO_4)_2(OH)_6$), hydronium jarosite
1184 ($(H_3O)Fe^{3+}_3(SO_4)_2(OH)_6$)) are shown here as "jarosite". Big circles indicate major
1185 quantities of that mineral and small circles indicate minor abundances.

ACCEPTED MANUSCRIPT

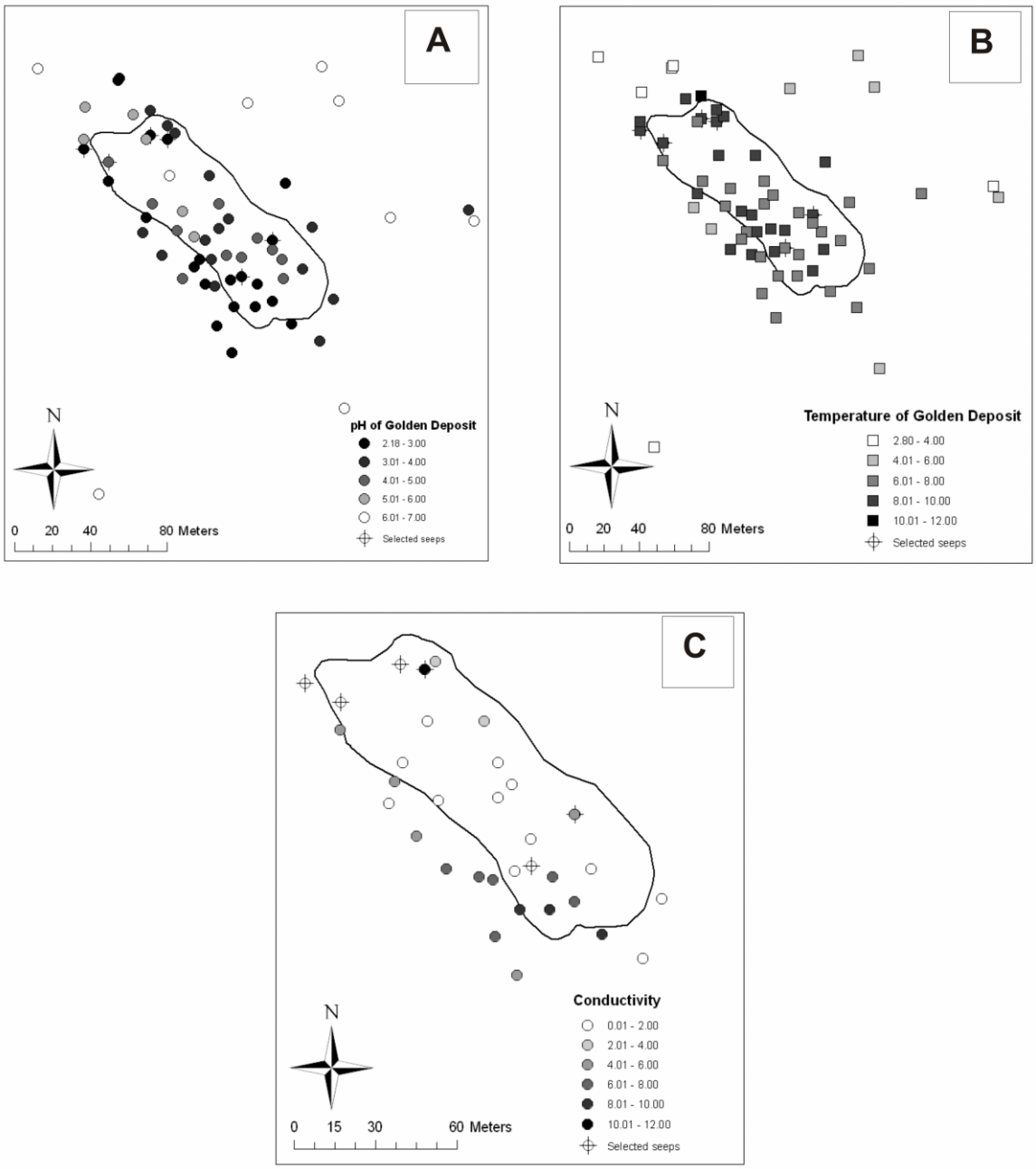

Fig. 5. A. pH map of the Golden Deposit; B. Map of water temperatures (reported in °C); C. Conductivity map (reported in mS/cm).

ACCEPTED MANUSCRIPT

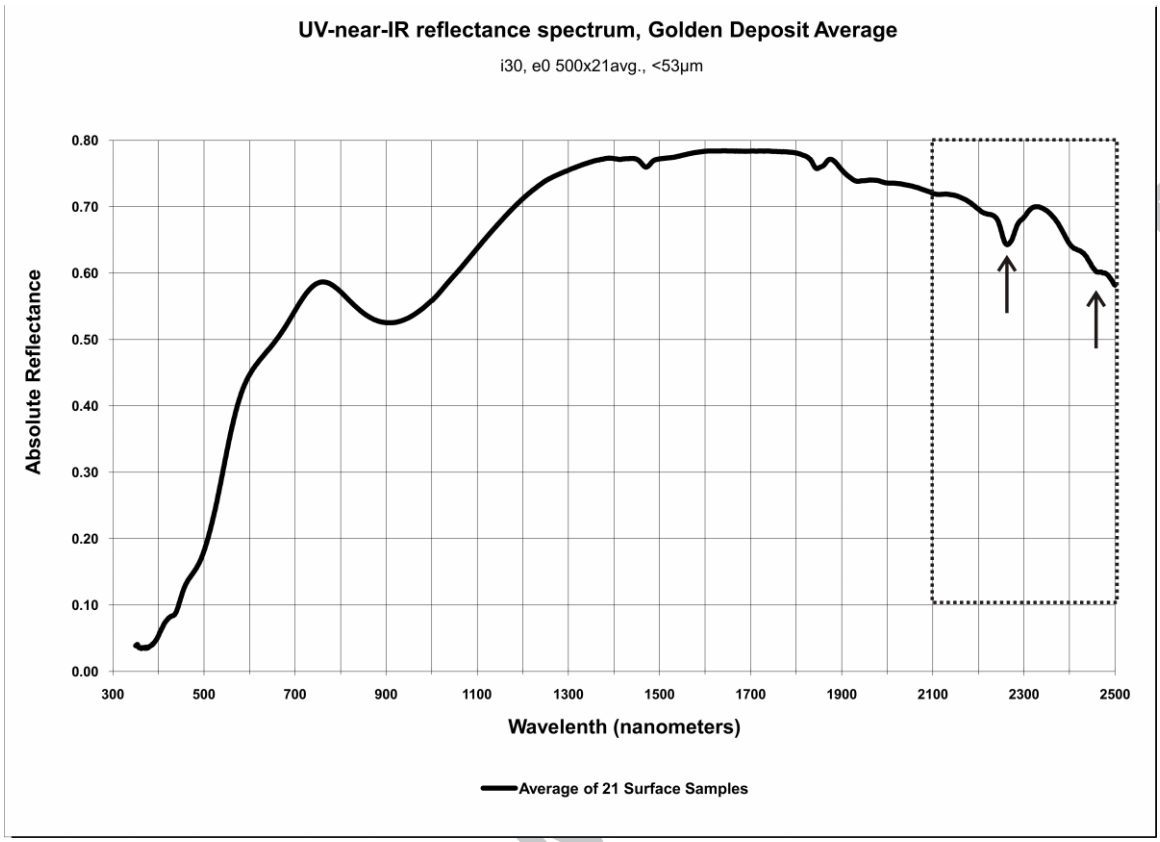

Fig. 6. Representative Ultraviolet-visible-near-infrared reflectance spectrum of the GD, to simulate perspective of an orbital instrument. Average obtained via a linear mixture of the spectra of 21 of the surficial samples (ochres and crusts). Jarosite masks all other minerals. Arrows indicate absorption features centered at 2.265 and 2.46 µm, which correspond to absorption features in the Mawrth Vallis spectra shown in Figure 7, and rectangle indicates spectral range shown in Figure 7.

ACCEPTED MANUSCRIPT

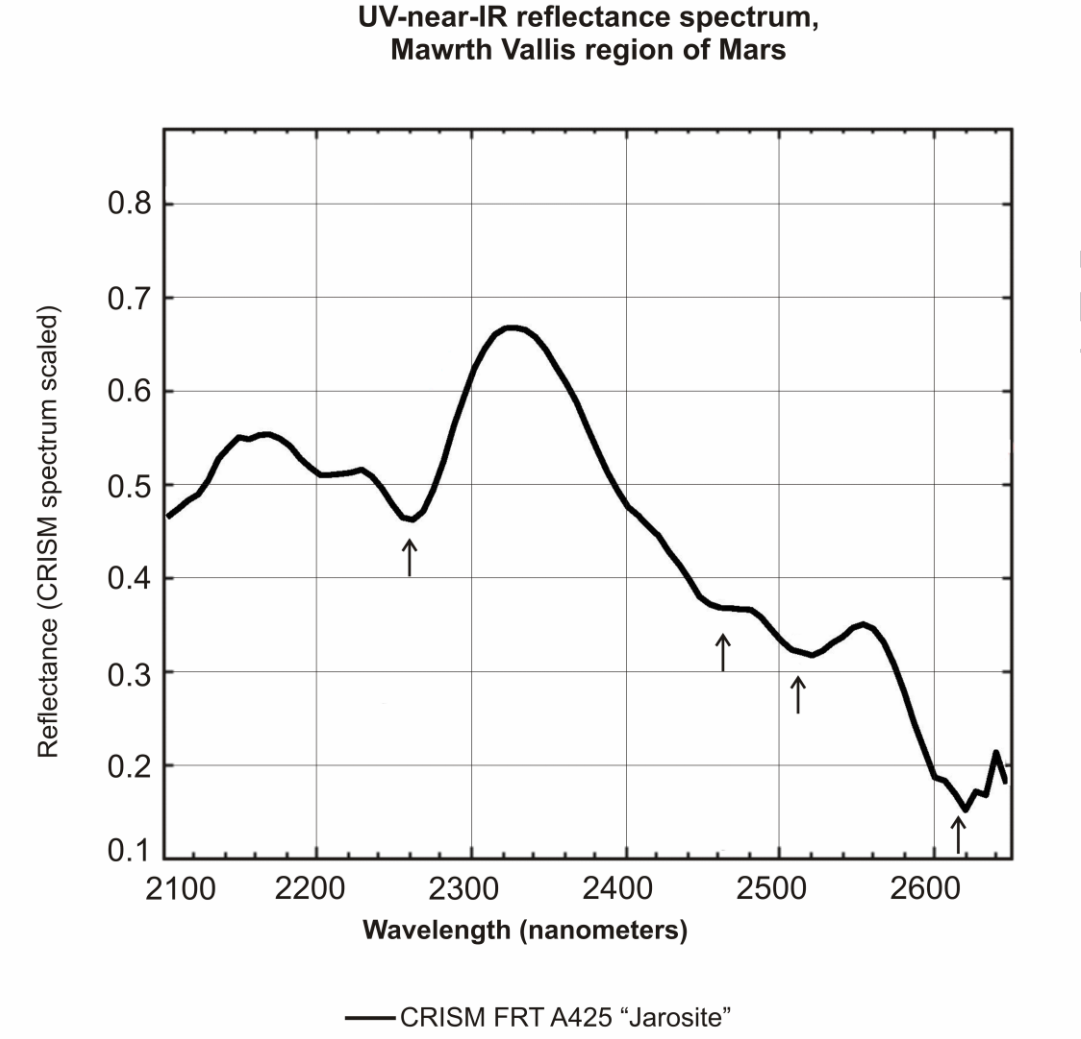

Fig. 7. Smoothed CRISM spectrum from the ovoid jarosite deposit in Mawrth Vallis (modified from Farrand et al., 2009). Note absorption features centered at 2.265 and 2.46 µm, which correspond to absorption features in the GD spectra shown in Figure 6. FRT refers to the fact that spatial resolution of this spectrum is in "full resolution targeted" mode, at 15–19 m/pixel.

ACCEPTED MANUSCRIPT

Table 1

Comparisons between properties of the Golden Deposit, Canada; Eagle Plains, Canada; and Rio Tinto, Spain, to Meridiani Planum and Mawrth Vallis, Mars, at the time of jarosite deposition. "++" indicates prominently featured at that side, "+" indicates present in lesser quantities, "-" indicates not present, and "?" indicates unknown.

Property	Golden Deposit	Eagle Plains[b]	Rio Tinto[c]	Meridiani Planum[g]	Mawrth Vallis[h]
Jarosite	++	+	+	+	++
Other sulfates	++	++	++	++	++
Hematite	+	+	+	++	-
Goethite	+	+	+	+	+
Salts (ionic strength)	++	+	++	++	?
Microorganisms	+	+	++	?	?
Permafrost	+	+	-	+ (?)	+ (?)
pH	2-6	2-5	2-3	<4 (?)	2-4 (?)
Water temperature	2-10 °C	3-12 °C	10 °C, constant	?	?
Conductivity	0.01-10 mS cm-1	30-4000 mS cm-1	1.95-1500 mS cm-1[d,e]	?	?
Latitude	65.2° N	66.4° N	37.2° N	0.2° N	22.3° N
Mean annual air temperature	-5.52 °C[a] (Norman Wells)	-4.1 ± 3.8 °C	17.5 ºC[f]	-60 ºC[i] (today)	-65 ºC[i] (today)
Max/min air temperature	35/-52 °C[a] (Norman Wells)	33/-59 °C[k] (Old Crow, 67.6° N)	40/0 °C	22/-98 °C[j] (today)	?
Mean annual precipitation	290 mm[a] (Norman Wells)	380 mm	760 mm[f]	trace (?) (today)	trace (?) (today)

[a]Environment Canada, (2010a); [b]Lacelle and Leveille, (2010); [c]Amils et al., (2007); [d]Buckby et al., (2003); [e]Hudson-Edwards et al., (1999); [f]Bonaccorsci et al., (2008); [g]Squyres et al., (2004a); [h]Farrand et al., (2009); [i]Mellon and Phillips, (2001); [j]Spanovich et al., (2006); [k]Environment Canada, (2010b).

ACCEPTED MANUSCRIPT

Table 2

Mineralogy of 43 samples from the GD. "X" indicates mineral comprises a major portion of sample, "x" a minor portion, based on qualitative XRD peak height intensities. Established symbols used where possible (Kretz, 1983). Njrs = natrojarosite ($NaFe^{3+}_3(SO_4)_2(OH)_6$), Jrs = jarosite ($KFe^{3+}_3(SO_4)_2(OH)_6$), Hjrs = hydronium jarosite ($(H_3O)Fe^{3+}_3(SO_4)_2(OH)_6$), Gt = goethite ($Fe^{3+}O(OH)$), Gp = gypsum ($CaSO_4{\cdot}2H_2O$), Hem = hematite ($Fe_2O_3$), Qtz = quartz, Pl = plagioclase, Rt = rutile, Ms = muscovite, Ill = illite, Gis = gismondine. Also ferrihydrite ($Fe_5O_7(OH)\cdot 4H_2O$), anhydrite ($CaSO_4$), hexahydrite ($MgSO_4{\cdot}6H_2O$), thenardite (Na_2SO_4), vauxite ($Fe^{2+}Al_2(PO_4)_2(OH)_2{\cdot}6(H_2O)$), fibroferrite ($Fe^{3+}(SO_4)(OH){\cdot}5(H_2O)$), alunogen ($Al_2(SO_4)_3{\cdot}17H_2O$), nacrite ($Al_2Si_2O_5(OH)_4$), and douglasite ($K_2Fe^{2+}Cl_4{\cdot}2H_2O$).

Sample Type	Sample # (NW to SE)	Njrs	Jrs	Hjrs	Gt	Gp	Hem	Qtz	Pl	Rt	Ms	Ill	Gis	Other minerals
ochre	GD-site5	X	X	X	x	x	x	X		x	x	x		
ochre	GD-16b	X	X		x	x		x	x	x	x			
ochre	GD-site4	X	X		x			x	x	x	x			
ochre	GD-site3a	X	X	X	x			x	x	x	x			
ochre	GD-site2c	X	X	X	x	x	x	x		x	x	x		
ochre	GD-site2d	X	X	X	x	x	x	x		x	x	x		
ochre	GD-23	X	X		x			x	x	x	x			
ochre	GD-13b	X	X		x			X		x	x			
ochre	GD-24 (st 1)	X	X		x		x	X		x	x			
ochre	GD-04 (p 2)	X	X		x			x						
ochre	GD-03a	X	X	X	x			x						
crust	GD-12	X	X	X	x			x		x	x			
crust	GD-11	X			X			X	x		x			
crust	GD-10a	X	X		x			X						
crust	GD-10b	X	X		x			X	x		x			
core, 0cm	GD-site2a	X	X	X	x	x	x	x		x	x	x		
core, 10 cm	GD-site2b	X	X	X	x	x	x	x		x	x	x		
core, 40 cm	GD-site2f	X	X	X	X	X	x	X	x	x	x	x		
core, 50 cm	GD-site2e	X	X	X	x	x	x	X	x	x	x	x		
transect	GD-T4a	X	X	X	x			X	x	x	x			
transect	GD-T4b		x		x			X	x	x	x			
transect	GD-T4c				x			X	x	x	x		x	
transect	GD-T3a	x	x	x	x			X	x	x	x			
transect	GD-14		x		x			X	x	x	x			
transect	GD-15	X	X		x	x	x	X		x	x			
transect	GD-T2c		x		x			X	x	x	x			
transect	GD-T2e	x	x	x	x			X	x	x	x			
transect	GD-T1a	x	x		x			X	x	x	x		x	
transect	GD-T5c	x	x	x	x		x	X		x	x			Ferrihydrite
transect	GD-T5e		x	X	x	x		x	x	x	x		x	
transect	GD-T5g		x	X	x	x		x	x	x	x		x	
transect	GD-21							X	x	x	x			Anhydrite
transect	GD-22			x	X		x	X	x	x	x			
terrace	GD-19	x	x		x			X	x	x	x			
terrace	GD-20	X	x		x			X	x	x	x			
evaporite	GD-01					X								
evaporite	GD-02					X								
evaporite	GD-03					x								Hexahydrite, thenardite, vauxite, fibroferrite
shale	GD-25		x					X			x	x		
shale	GD-26b		x					X			x			
shale	GD-26d				x		x	X	x	x	x			
shale	GD-pit2a	X	X		x			X			x			Alunogen, nacrite, douglasite
shale	GD-pit2b				x		x	X			x	x		Nacrite, alunogen

ACCEPTED MANUSCRIPT

Table 3

ICP-ES major oxide and trace element results ($LiBO_2/Li_2B_4O_7$ fusion ICP-ES analysis) from Acme Analytical Laboratories, Ltd. Total Fe is reported as Fe_2O_3. Reported in weight % or ppm as indicated.

Analyte	SiO_2	Al_2O_3	Fe_2O_3	MgO	CaO	Na_2O	K_2O	TiO_2	P_2O_5	MnO	Cr_2O_3
Unit	%	%	%	%	%	%	%	%	%	%	%
MDL	0.01	0.01	0.04	0.01	0.01	0.01	0.01	0.01	0.01	0.01	0.002
Sample											
GD-23	11.39	1.48	47.13	0.08	0.03	2.34	2.32	0.10	0.07	<0.01	0.004
GD-10a	14.77	1.73	45.00	0.09	0.07	2.33	2.31	0.14	0.06	<0.01	0.003
GD-site2a	8.22	0.96	50.10	0.09	0.03	2.29	3.37	0.08	0.06	<0.01	0.006
GD-site2f	10.74	1.12	50.30	0.06	0.12	1.92	3.41	0.11	0.07	<0.01	<0.002
GD-T4a	23.73	4.38	39.97	0.28	0.09	1.54	2.19	0.28	0.10	0.02	0.005
GD-T4c	38.80	9.88	19.24	0.62	0.59	0.43	1.42	0.37	0.30	0.09	0.010

Analyte	Ba	Ni	Sr	Zr	Y	Nb	Sc	LOI	Sum	TOT/C	TOT/S
Unit	PPM	PPM	PPM	PPM	PPM	PPM	PPM	%	%	%	%
MDL	5	20	2	5	3	5	1	-5.1	0.01	0.02	0.02
continued...											
Sample											
GD-23	192	<20	39	37	<3	<5	2	35.0	99.98	1.25	8.73
GD-10a	207	<20	42	88	4	<5	2	33.4	99.96	0.79	8.39
GD-site2a	133	37	35	41	3	14	1	34.8	99.99	0.73	9.82
GD-site2f	159	<20	41	85	4	<5	1	32.1	99.99	0.70	8.67
GD-T4a	373	<20	56	121	10	<5	4	27.3	99.98	1.48	5.05
GD-T4c	525	24	68	187	28	7	15	28.1	99.94	8.54	0.21

ACCEPTED MANUSCRIPT

ACCEPTED MANUSCRIPT

Table 4

Water chemistry data for Sites 1-5 and Pond 2, as measured by the Environment Canada, Pacific Environmental Science Centre (PESC) in Vancouver, Canada.

	Alkalinity, Total	Chloride (Cl)	Fluoride (F)	**Sulfate (SO_4)**	**pH**	Conductivity	Aluminum (Al)	Antimony (Sb)
	mg CaCO3/L	*mg/L*	*mg/L*	***mg/L***		*µS/cm*	*mg/L*	*mg/L*
Pond 2	16.20	2.10	0.07	**743.00**	**6.67**	1320.00	0.19	0.05
Site 1	< 0.5	1.30	0.08	**305.00**	**4.14**	616.00	1.86	< 0.05
Site 2	< 0.5	18.30	0.17	**4170.00**	**2.78**	6300.00	1.07	0.39
Site 3	< 0.5	3.60	< 0.01	**2770.00**	**3.07**	4260.00	16.90	0.23
Site 4	0.60	1.00	0.17	**148.00**	**5.23**	354.00	1.42	< 0.05
Site 5	< 0.5	0.70	0.08	**111.00**	**4.04**	274.00	0.50	< 0.05
MEAN	**8.40**	**4.50**	**0.11**	**1374.50**	**4.32**	**2187.33**	**3.66**	**0.22**
MEDIAN	**8.40**	**1.70**	**0.08**	**524.00**	**4.09**	**968.00**	**1.25**	**0.23**
MAX	**16.20**	**18.30**	**0.17**	**4170.00**	**6.67**	**6300.00**	**16.90**	**0.39**
MIN	**<0.50**	**0.70**	**0.07**	**111.00**	**2.78**	**274.00**	**0.19**	**<0.05**

	Boron (B)	Calcium (Ca)	**Iron (Fe)**	Magnesium (Mg)	Manganese (Mn)	Phosphorus (P)	**Potassium (K)**	Silicon (Si)
	mg/L	*mg/L*	***mg/L***	*mg/L*	*mg/L*	*mg/L*	***mg/L***	*mg/L*
Pond 2	0.06	91.40	**8.49**	84.40	0.74	1.20	**3.80**	4.23
Site 1	0.02	29.50	**7.08**	40.10	0.65	0.60	**0.50**	4.44
Site 2	0.52	343.00	**309.00**	475.00	4.19	2.80	**20.10**	14.10
Site 3	0.32	227.00	**11.30**	373.00	3.98	2.30	**0.90**	19.50
Site 4	0.01	20.00	**5.81**	26.20	0.45	0.40	**0.30**	4.04
Site 5	< 0.01	14.90	**18.40**	12.10	0.13	0.20	**0.30**	3.17
MEAN	**0.19**	**120.97**	**60.01**	**168.47**	**1.69**	**1.25**	**4.32**	**8.25**
MEDIAN	**0.06**	**60.45**	**9.90**	**62.25**	**0.69**	**0.90**	**0.70**	**4.34**
MAX	**0.52**	**343.00**	**309.00**	**475.00**	**4.19**	**2.80**	**20.10**	**19.50**
MIN	**<0.01**	**14.90**	**5.81**	**12.10**	**0.13**	**0.20**	**0.30**	**3.17**

	Sodium (Na)	Strontium (Sr)	**Sulfur (S)**	Hardness, Dissolved total - calc.	*DIC	DOC	TN	TP
	mg/L	*mg/L*	***mg/L***	*mg/L*	*mg/L*	*mg/L*	*mg/L*	*mg/L*
Pond 2	**80.70**	0.04	**239.00**	593.00	5.00	9.80	1.76	0.01
Site 1	**19.20**	0.02	**100.00**	260.00	< 0.5	17.20	1.27	0.01
Site 2	**426.00**	0.04	**1596.00**	3370.00	0.60	6.20	15.30	0.01
Site 3	**322.00**	0.05	**1030.00**	2190.00	0.60	13.60	8.82	0.01
Site 4	**7.40**	0.02	**57.80**	174.00	< 0.5	22.90	0.90	0.01
Site 5	**2.90**	0.02	**27.80**	122.00	0.80	11.70	1.58	0.02
MEAN	**143.03**	**0.03**	**508.43**	**1118.17**	**1.75**	**13.57**	**4.94**	**0.01**
MEDIAN	**49.95**	**0.03**	**169.50**	**426.50**	**0.70**	**12.65**	**1.67**	**0.01**
MAX	**426.00**	**0.05**	**1596.00**	**3370.00**	**5.00**	**22.90**	**15.30**	**0.02**
MIN	**2.90**	**0.02**	**27.80**	**122.00**	**0.60**	**6.20**	**0.90**	**0.01**

Figure 1

ACCEPTED MANUSCRIPT

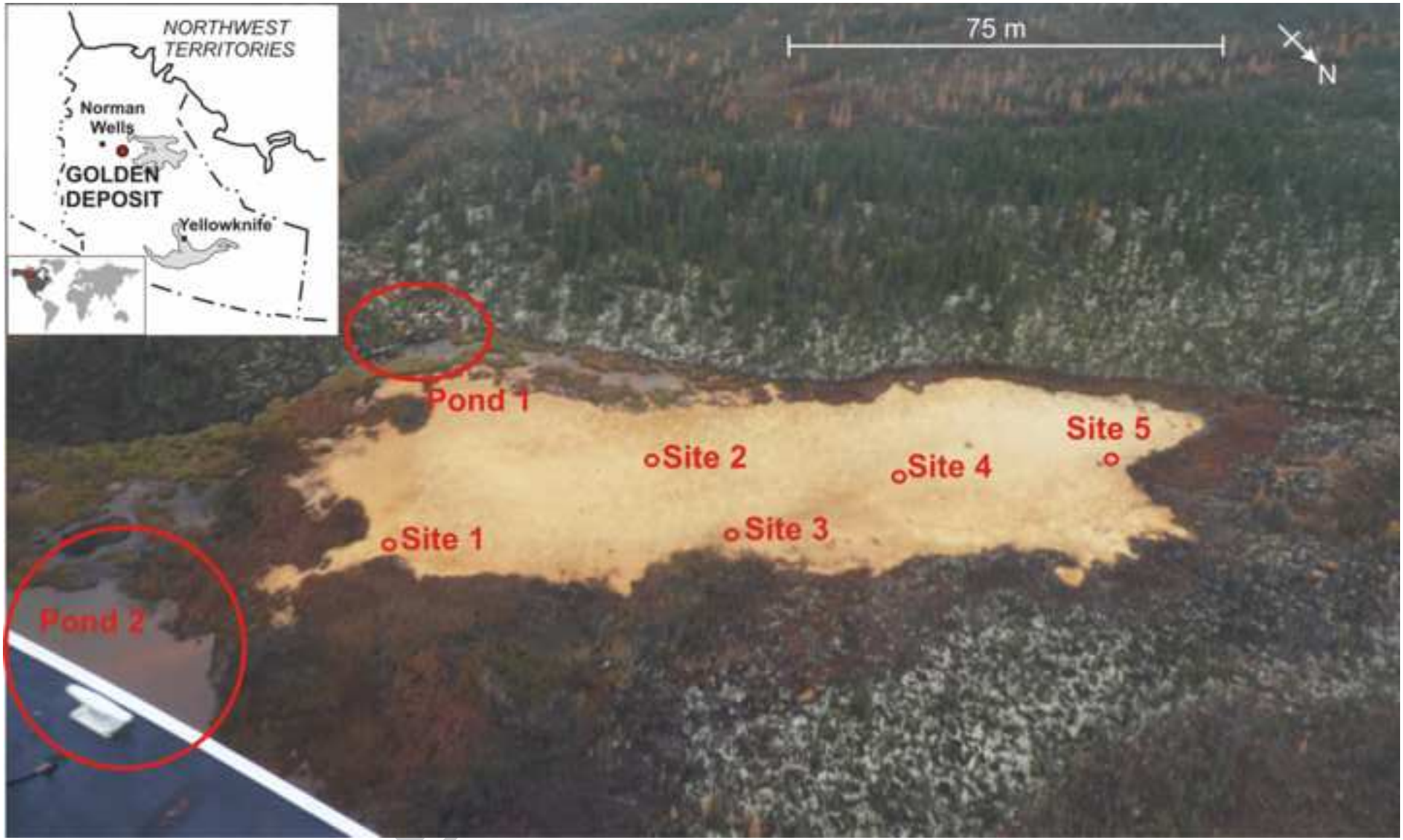

Figure 2

ACCEPTED MANUSCRIPT

Figure 3

ACCEPTED MANUSCRIPT

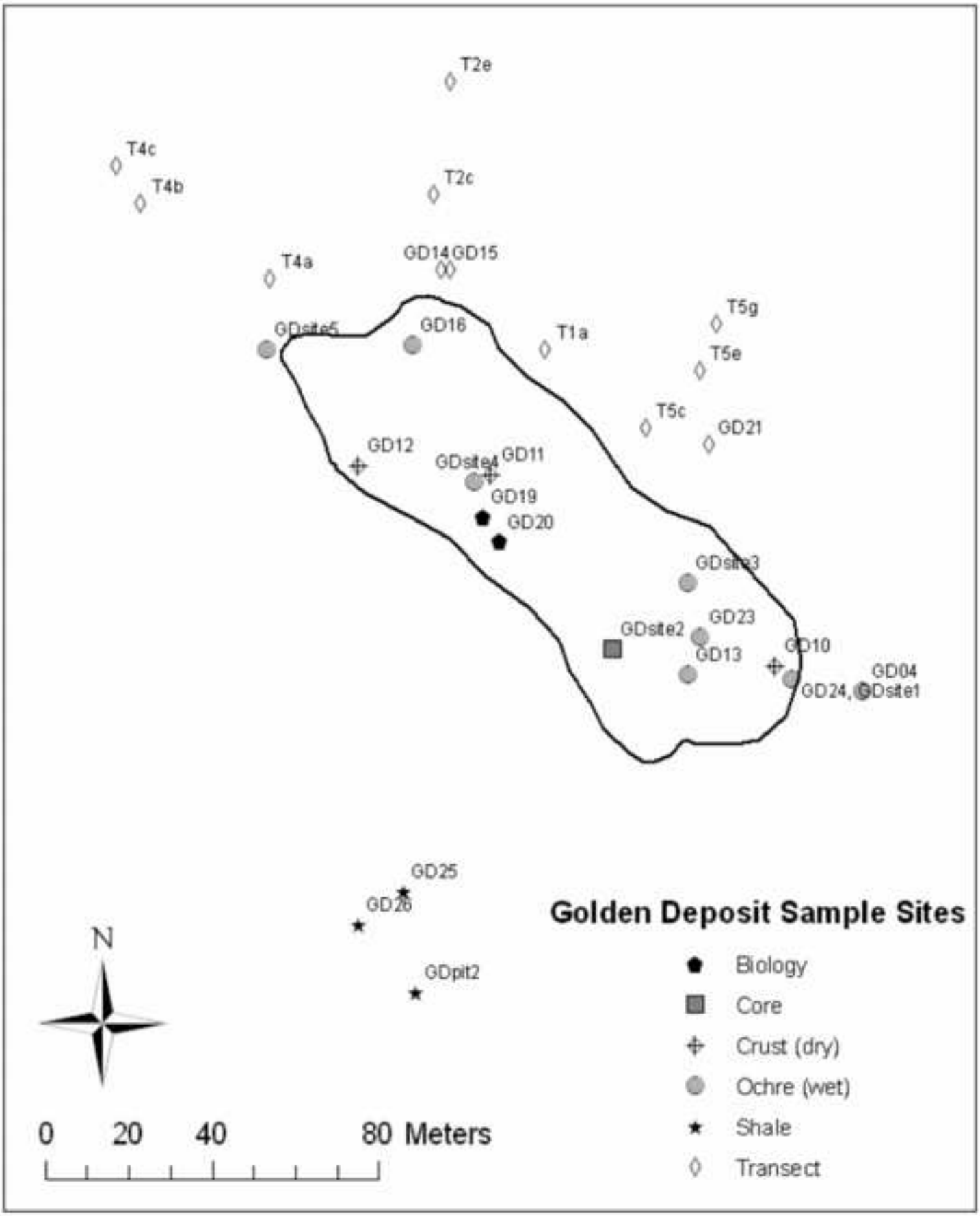

Figure 4

ACCEPTED MANUSCRIPT

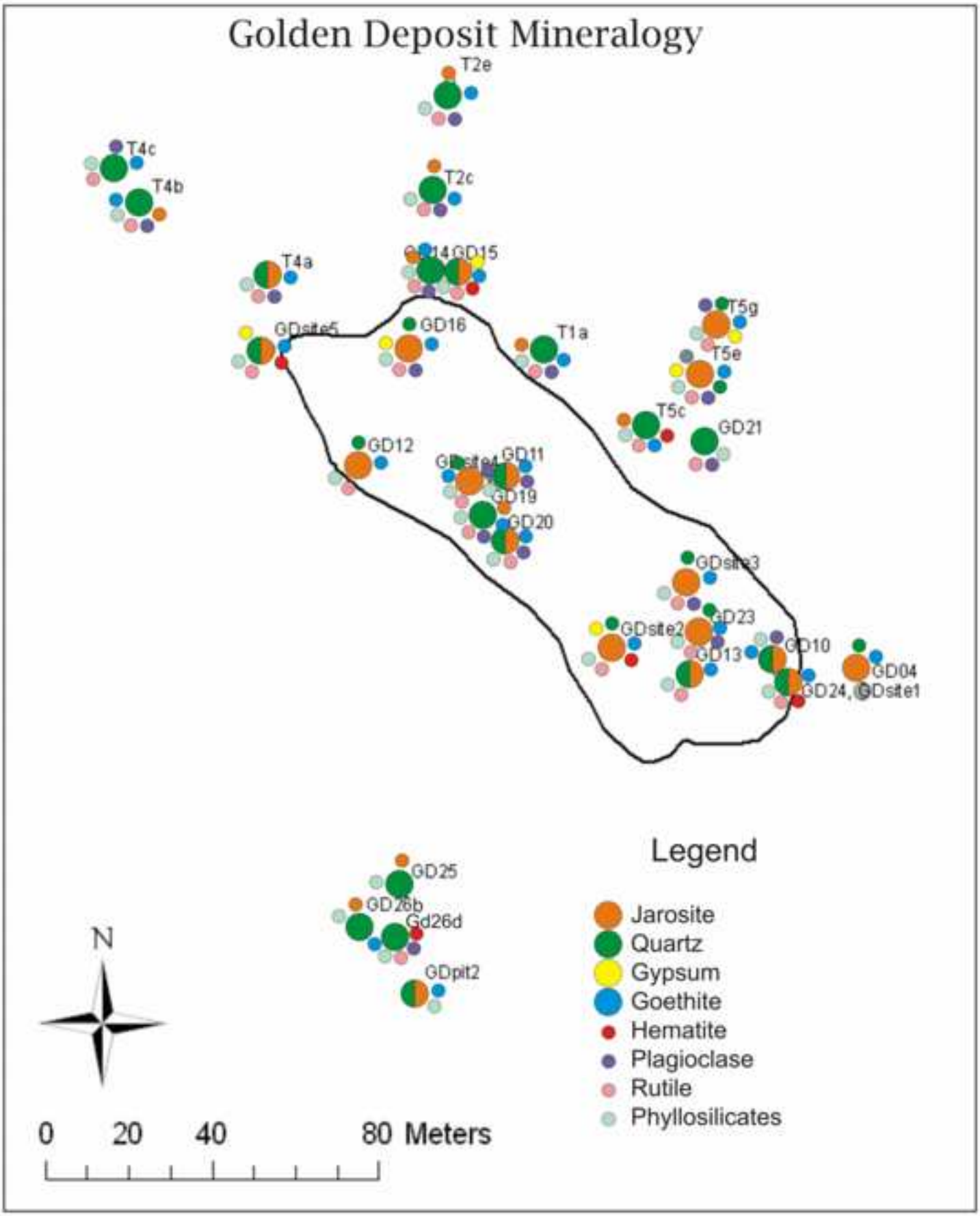

Figure 5

ACCEPTED MANUSCRIPT

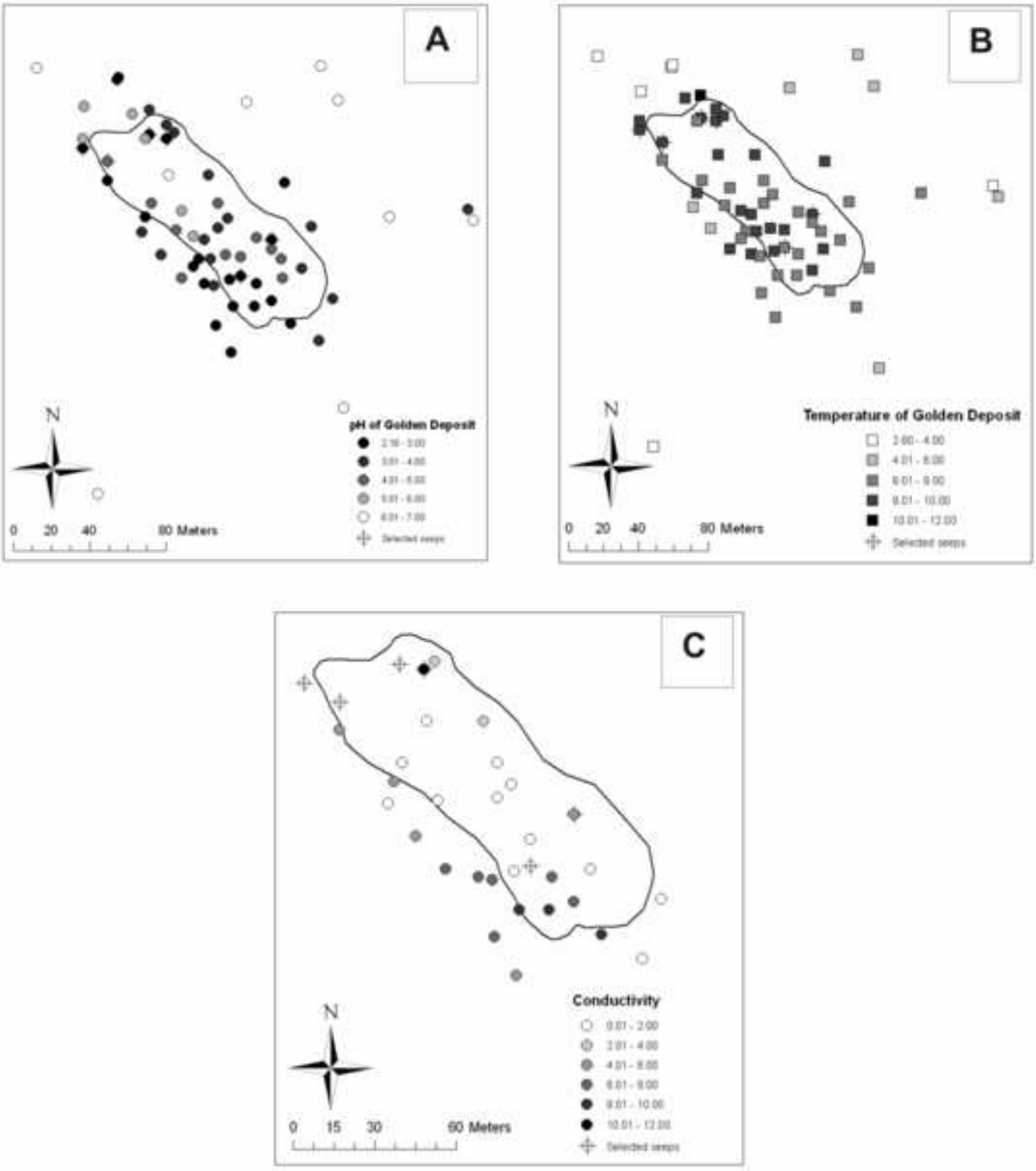

Figure 6

ACCEPTED MANUSCRIPT

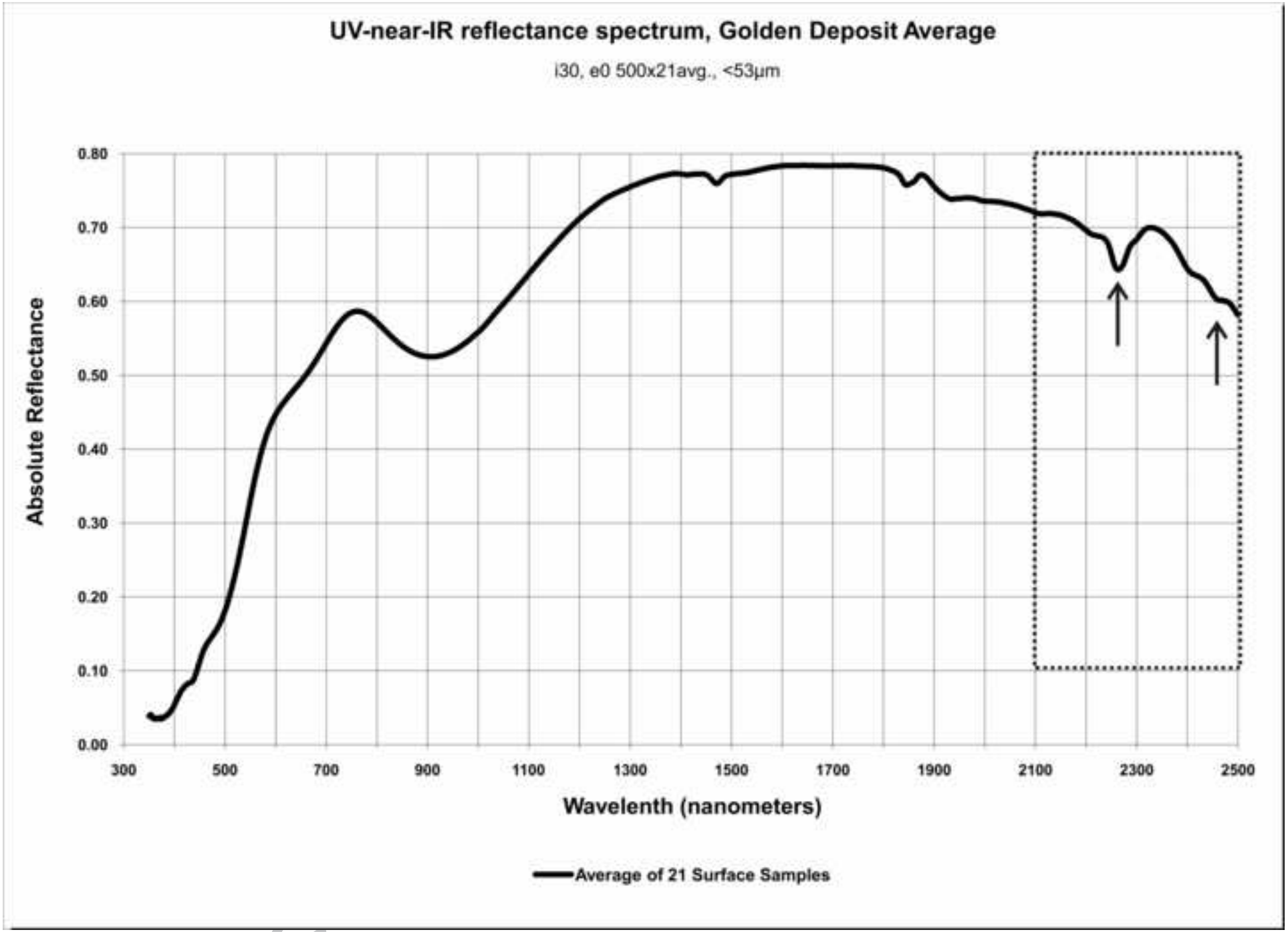

Figure 7

ACCEPTED MANUSCRIPT

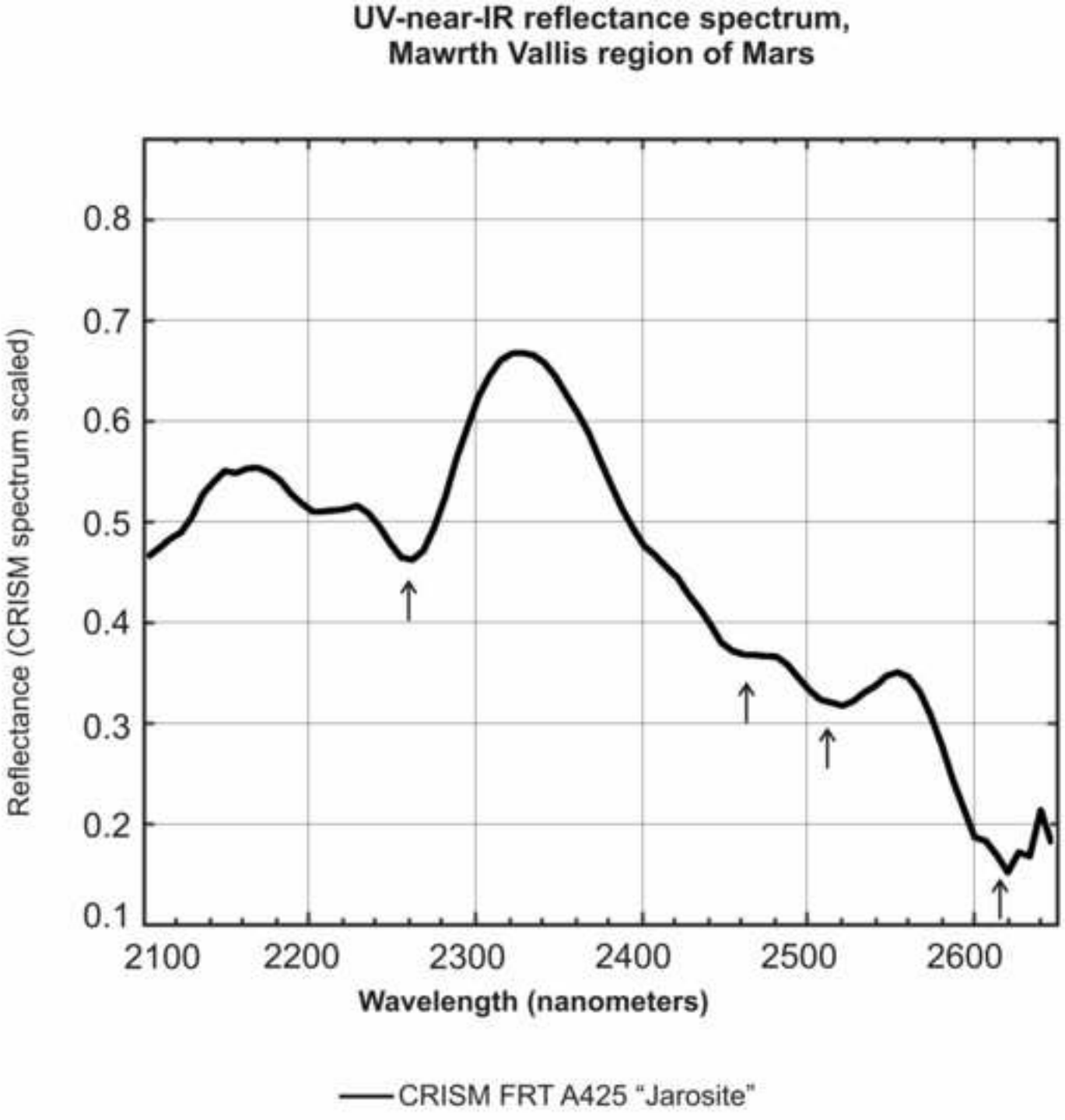

ACCEPTED MANUSCRIPT

Highlights

- There is evidence for jarosite at Meridiani Planum and Mawrth Vallis, Mars
- Depositional mechanisms for jarosite on Mars are not known
- The cold seep emplaced jarositic Golden Deposit serves as a depositional analogue
- Mineralogy and spectral of the GD jarosite are analogous to Martian deposits
- Jarosite is stable on Mars and may preserve evidence of paleoenvironments or life

ACCEPTED MANUSCRIPT